Working Fluid Design for Organic Rankine Cycle (ORC) Systems

Akshay Hattiangadi

Master of Science Thesis

TU Delft Delft University of Technology

Mechanical, Maritime and Materials Engineering

Working Fluid Design for Organic Rankine Cycle (ORC) Systems

Master of Science Thesis

For the degree of Master of Science in Sustainable Energy Technology
at Delft University of Technology

Akshay Hattiangadi

August 7, 2013

Faculty of Applied Sciences (TNW) · Delft University of Technology

Delft University of Technology
Department of
Energy Technology, Process and Energy (et)

The undersigned hereby certify that they have read and recommend to the Faculty of Applied Sciences (TNW) for acceptance a thesis entitled

Working Fluid Design for Organic Rankine Cycle (ORC) Systems

by

Akshay Hattiangadi

in partial fulfillment of the requirements for the degree of

Master of Science Sustainable Energy Technology

Dated: August 7, 2013

Supervisor(s):

Prof.dr.ir. P. Colonna

ir. T. Mathijssen

Reader(s):

Prof.dr.ir. F. van Keulen

ir. T. P. van der Stelt

Abstract

The Organic Rankine Cycle is an energy conversion cycle similar to the conventional Rankine cycle which runs on a working fluid other than water. The selection of a working fluid is a critical part of designing an Organic Rankine Cycle (ORC) system. The number of fluid types actually used in commercial ORC power plants do not justify the number of fluid selection studies present in scientific literature. Hence the objective of this work is to develop a tool which simultaneously optimizes the energy conversion process and selects the optimum working fluid for a given heat source. It is based on a framework that uses a continuous-molecular targeting approach which allows for an integrated working fluid and system design. The process is modeled in Cycle Tempo, a modern graphical tool for thermodynamic analysis and optimization of systems for the production of electricity, heat and refrigeration. The system is simultaneously optimized with the pure component parameters of PCP-SAFT equation of state using a state-of-the-art optimization suite. The working fluid is selected by comparison of the pure component parameters of the PCP-SAFT equation of state with real fluids. A preliminary turbine model implemented directs the tool to generate suitable fluids for practically realistic systems.

The tool has been tested for a waste heat recovery system for heavy-duty truck engines based on an ORC turbogenerator. The choice of working fluid is restricted to only the siloxane class which not only adheres to the technical, environmental, and toxicological requirements typical of the automotive sector but also allows for the implementation of a preliminary radial turbine model, whose shaft can be lubricated by the working fluid itself. The turbine has been modeled by applying the methodology of using non-dimensional parameters. Future work will be devoted to implement detailed component models and extending the scope of fluid selection to other organic fluid classes.

Table of Contents

List of Figures

List of Tables

Acknowledgements

First of all, I would like to sincerely thank my supervisor, Prof. Dr. Piero Colonna. I consider myself lucky to have had you as my supervisor; without your attention, enthusiasm and guidance my work would most likely not have been productive. Your approach towards problem solving and defining the project scope prevented me from wandering away from my objective.

My sincere thanks to my daily supervisor Tiemo Mathijssen, who was always available to help me out during the last 8 months. I greatly appreciate your willingness to discuss even the smallest of problems with me during the course of this work. I would also like to thank Teus van der Stelt who guided me through the tough times of figuring out the programming logic and debugging the tool. I would have been truly lost if not for your support.

I am grateful to Dr. André Bardow and Matthias Lampe for their support, hospitality and discussions on defining the constrains for the optimization problem in this work. I truly enjoyed the two weeks I spent at Lehrstuhl für Technische Thermodynamik, RWTH Aachen and I would like to thank Dr. Piero Colonna and Dr. André Bardow for offering me the possibility to do this. Many thanks to Dr. David Pasquale for providing me with the license for the Nexus optimization suite and supporting me with the software. I truly appreciate your constant support and accessibility via Skype even on weekends. A special word of gratitude to Luca and the iChrome support team for their constant help in solving the problems related to the optimization suite.

I am grateful to Juan Sebastian Bahamonde for his help with the turbine model and clearing my doubts. I would also like to thank Dr. Wolfgang Lang, SES-Tec OG, Austria and Emiliano Casati for devoting their time and helping me with the turbine model implementation. I would like to thank all my friends and colleagues in TU Delft and India for their constant support, encouragement and enjoyable moments spent together.

I want to express my gratitude to the rest of the examination committee. I appreciate their time devoted to reading and evaluating this document.

Finally, I want to thank my family for their love and support throughout the duration of this masters.

Delft, University of Technology — Akshay Hattiangadi

August 7, 2013

Chapter 1

Introduction

The energy industry has arguably been one of the primary drivers for the world's growing economies from the early twentieth century to the present. The strive to become energy independent and meet the demand has increased the dependence on fossil fuels leading to climate change. While the mandate of the energy industry in the twentieth century was to provide power to consumers, anywhere, anytime and at an affordable price, the mandate as we progress in the second decade of the twenty-first century is much more complex, demanding not only reliable but cleaner and more efficient power. With the concentration of carbon dioxide in the atmosphere recently touching the milestone level of 400 parts per million (ppm)[2], efforts are being made to develop new renewable technologies such as solar, wind or geothermal power. But the penetration of these technologies into the energy market is relatively small compared to the conventional sources of energy. Additionally, the highly energy intensive industrial installations reject heat which accounts for more than 50% of the heat generated [3].

With reports on Germany switching to coal-fired (albeit cleaner coal) in order to compensate for the shutting down of the nuclear power stations [4], the need of the hour is to find a technology which can serve as a "bridge to the future". This transition technology should not only accelerate the process of implementation of the clean and new technologies but also address the requirements of industrial heat recovery. Conventional steam power cycles has its limitations in recovering low grade waste heat. It is thus necessary to analyze other possibilities which can serve such purpose. Organic Rankine Cycle (ORC) is one such technology which is ideally suited for this application. The following section introduces the ORC technology.

1-1 Organic Rankine Cycle

ORC is a promising technology which involves conversion of heat from any source including renewable sources like solar, geothermal, biomass, etc or waste heat to power[5]. The system is similar to the conventional Rankine cycle except for some differences, the major being the

working fluid which is an organic fluid replacing the conventionally used steam/water. This fluid is vaporized in the vapor generator or heat recovery boiler wherein the three phases of heating a fluid viz. preheating, vaporization and super-heating take place in a single heat exchanger. The vaporized fluid is then expanded in a turbine. Variations in the cycle architecture such as reheating and turbine bleeding are generally not suitable for ORC systems [6]. The expanded working fluid which is still a superheated vapor in such cases is cooled to within the range of its condensing temperature in a recuperator. The condenser then condenses the partially cooled vapor which is subsequently pumped to the evaporator via the recuperator which preheats the fluid. ORC finds its major application in waste heat recovery from flue gas and hence DiBella et. al. [7] suggests that the recuperator not only improves the cycle efficiency but it also maintains the minimum fluid temperature required by the vapor generator to prevent corrosion due to condensation of sulfur from the exhaust gas.

Figure 1-1 illustrates a typical ORC system with recuperation.

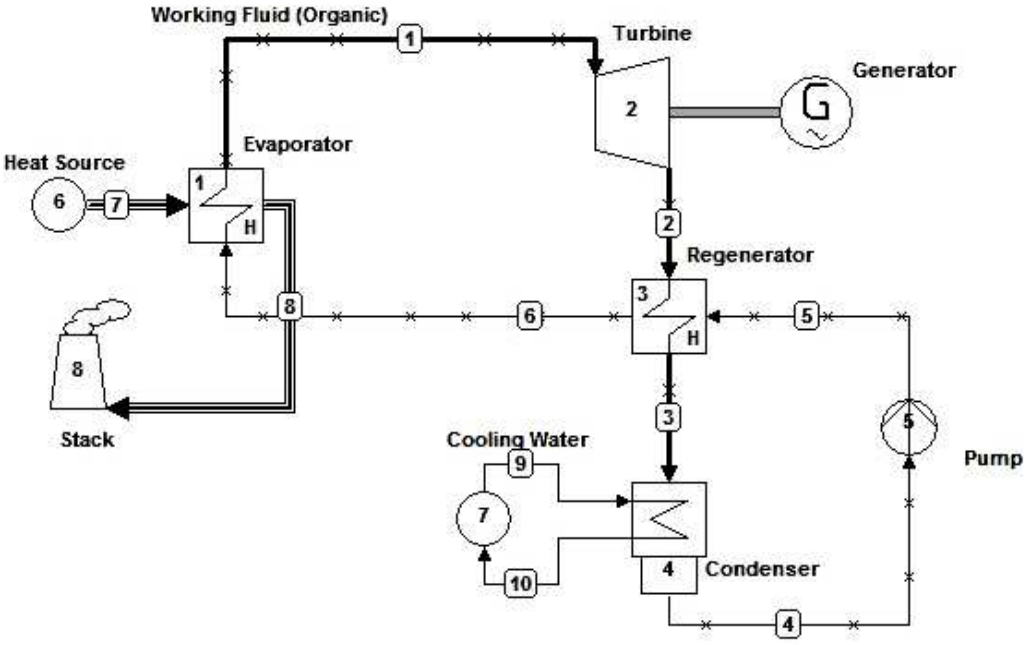

Figure 1-1: Layout of an ORC system [8]

The following section provides a summary of the comparison between ORC and steam rankine cycle.

1-1-1 Comparison with Water/Steam Rankine Cycle

ORC systems are quite similar in its layout to the conventional Rankine cycle with some differences which can serve both as an advantage and a disadvantage. According to Angelino et al. [9], configurations which are not feasible for water can be obtained with fluids having different critical parameters. The authors suggest low temperature supercritical cycles as one of its potential application. Quoilin et.al.[6], Vankeirsbilck et. al.[10], Tchanche et. al. [11]

and Chen et. al. [12] have done comprehensive reviews on the differences between ORC and conventional Rankine cycle systems. These are as follows:

Superheating : Figure 1-2 illustrates the major classification of fluids based on the slope of its vapor saturation curves. "Wet fluids" are those which have a negative slope. Water is classified as a wet fluid. Such fluids require superheating in order to avoid condensation during the expansion process. Ideal fluids for ORCs are generally either "Isentropic" or "Dry" with a zero or positive slope respectively which do not require superheating.

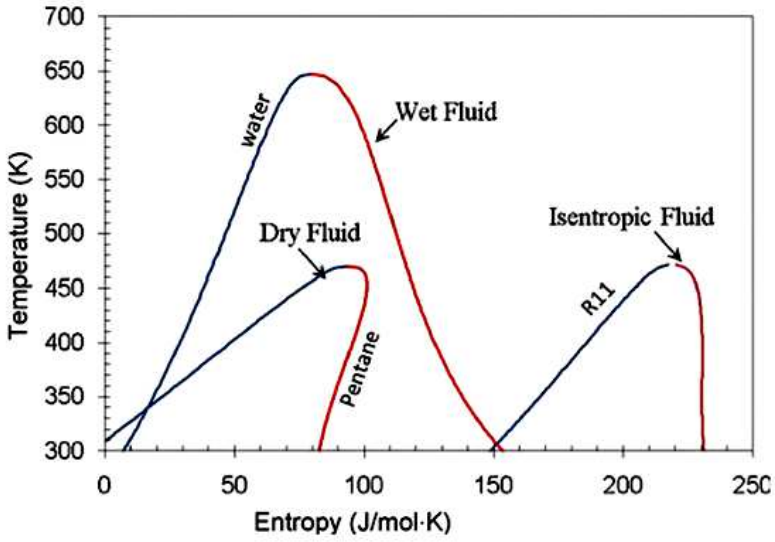

Figure 1-2: Three types of working fluids: dry, isentropic, and wet. Adapted from Chen et.al.[12]

The risk of blade erosion is thus reduced extending the lifetime of the expander to a considerable period of years.

Low temperature heat recovery : With its low boiling point, a properly selected organic working fluid can recover heat at much lower temperatures when compared to steam/water cycles (e.g. with geothermal sources).

Component size : ORC fluids have a high volumetric flow rate at the turbine outlet. Hence the size of the regenerator and condenser tends to be larger in such systems.

Boiler Design : ORC systems can use once-through boilers due to the relatively smaller density difference between vapor and liquid for the working fluids. Thus the use of boiler drums and the need to recirculate the fluid are avoided.

Turbine inlet temperature : Steam Rankine cycles require superheating and hence higher turbine inlet temperatures than an ORC system. This would require the use of expensive high temperature materials for the turbine blades and the boiler. In ORC systems, the turbine inlet temperatures are limited by the fluid's thermal stability limit.

Pump consumption : The amount of power consumed by the pump is proportional to the liquid volume flow rate and to the pressure difference between outlet and inlet. ORC systems have a higher volumetric flow rate and hence require relatively more pump power.

Maximum Cycle Pressure : The boiler in a steam cycle is usually subjected to high pressures of around 70 bar which increases the complexity and the costs [6]. ORC systems are generally used in small scale applications where compact plate-type heat exchangers are used which impose a technical limitation on the maximum pressure which is usually not more than 40 bar.

Working Fluid characteristics : Water as a working fluid is inexpensive, non-toxic, non-flammable, has low Global Warming Potential and zero Ozone Depleting Potential, chemically stable and low viscosity (and thus lower friction losses and higher heat exchange coefficients). However, a water-treatment and a deaerator must be integrated with the power plant to feed the cycle with high-purity deionized, oxygen free water. Organic fluids may be relatively toxic and is more expensive than water (excluding cost of pre-treatment). Chen et. al. [12] suggests that mass production or use of low cost hydrocarbon can reduce the costs.

Turbine design : The pressure ratio and the enthalpy drop over the turbine are very high in case of a steam cycle. As a consequence, turbines with several expansion stages are commonly used. In ORC cycles, the enthalpy drop is much lower, and hence a single or low number of stages in a turbine should suffice hence lowering the costs.

In summary, ORC presents a good business case for decentralized power generation typically of the order of less than a few MW. The modularity and versatility of this technology allows for the integration of ORC into currently used plants as a bottoming cycle. Some of the typical applications mentioned in reviews done by Vélez et.al [3], Tchanhe et. al [11], Chen et. al. [12], Quolin et.al. [6], Vankeirsbilck et. al. [10] are solar thermal systems, industrial waste heat recovery, biomass combined heat and power systems, ocean thermal energy conversion, geothermal applications, automotive waste heat recovery. For more details on these applications, the interested reader can refer to the references mentioned in the previous lines. The following section describes the current market scenario in ORC systems.

1-1-2 Market Scenario

Following the OPEC oil embargo in the 1970's, the need to research and develop alternative energy sources increased. ORC system manufacturers have been present in the market ever since due to this reason. Some of the major players are Turboden, ORMAT, Tri-o-gen and Enertime. Table 1-1 lists some of the ORC unit manufacturers.

The ORC market has been growing at an almost exponential rate. Figure 1-3 illustrates the evolution of installed power and the number of plants in operation, based on a compilation of manufacturer data. Figure 1-3 also reveals that ORC is a mature technology for waste heat recovery, biomass-CHP and geothermal power, but it is still niche for solar applications. Moreover, systems are mainly installed in the MW power range and very few ORC plants exist in the kW power range [6].

Table 1-1: Non-Exhaustive list of ORC system manufacturers (Adapted from Vélez F. et. al. [3] and Quoilin S. et. al. [6])

Manufacturer	Power Range [kW_e]	Heat Source Temperature [°C]	Applications	Technology
ORMAT, US	200-70000	150-300	Geothermal, WHR, Solar	Fluid: n-pentane Turbine: Two-stage axial Generator: Synchronous
Turboden, Italy	200-2000	100-300	Biomass-CHP, WHR, Geothermal	Fluids: OMTS, Solkatherm Turbine: Two-stage axial
Adoratec/Maxxtec, Germany	315-1600	300	Biomass-CHP	Fluid: OMTS
Opcon, Sweden	350-800	<120	WHR	Fluid: Ammonia Turbine: Lysholm
GMK, Germany	50-5000	120-350	WHR, Geothermal, Biomass-CHP	Turbine: Multi-stage axial
Bosch KWK, Germany	65-325	120-150	WHR	Fluid: R245fa
Turboden PureCycle, US	280	91-149	WHR, Geothermal	Fluid: R245fa Turbine: Radial inflow
GE CleanCycle	125	>121	WHR	Fluid: R245fa Turbine: Single stage radial inflow
Cryostar, France	N/A	100-400	WHR, Geothermal	Fluids: R245fa, R134a Turbine: Radial inflow
Tri-o-gen, Netherlands	160	>350	WHR	Fluid: Toluene Turbine: Radial turbo-expander
Electratherm, US	50	>93	WHR, Solar	Fluid: R245fa Expander: Twin screw
FREEPOWER , England	120	>110	Biomass-CHP, Solar, Geothermal	Turbine: High speed multi-stage axial
Infinity Turbine, US	10-50, >250	<90, 90-120	Geothermal, WHR	Fluid: R134a, R245fa
Barber Nichols, US	700, 2000, 2700	>115	Geothermal, WHR	N/A
Lti REEnergy, Germany	3	>160	WHR	N/A
Eneftech, Switzerland	5-10, 20-30	120 - 200	Geothermal, Biomass-CHP, Solar, WHR	Expander: Scroll
TransPacific Energy, US	100-5000	30-480	Solar, Geothermal, WHR	Fluid: TPE

Waste Heat Recovery (WHR),Combined Heat and Power (CHP)

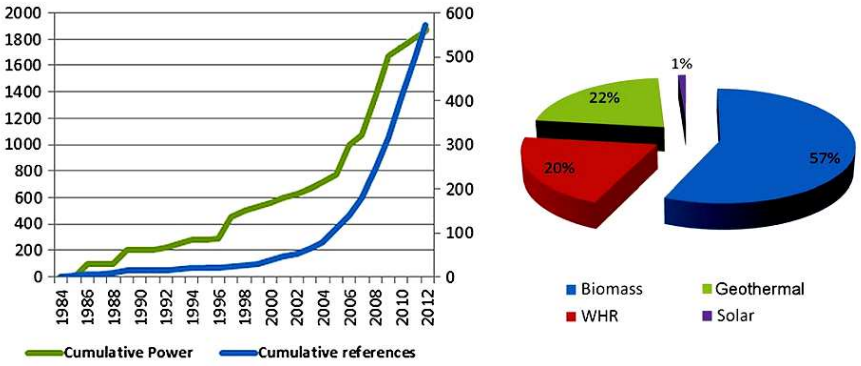

Figure 1-3: Market evolution (left) and share of each application in terms of number of units (right) (Adapted from Quoilin S. et. al.[6])

1-2 Motivation and Scope

One of the most important characteristics which determine the performance of an ORC system is the selection of the working fluid. The selected fluid should not only exhibit favorable physical, chemical, environmental, safety and economic properties such as low specific volume, viscosity, toxicity, flammability, ozone depletion potential (ODP), global warming potential (GWP) and cost but also contribute to favorable process attributes such as high efficiency or moderate pressure in heat exchangers [13].

Traditionally, the working fluid is selected by a trial and error procedure through experience of similar systems. A set of possible working fluid candidates are identified using heuristic knowledge about the process based on similar systems. These candidates are then assessed in a process simulation scheme and optimized [5]. Such an approach bears the risk to exclude the optimal working fluids from further consideration if the process objectives are

not considered in the initial screening step. This drawback can be successfully addressed through the use of Computer Aided Molecular Design (CAMD) in conjunction with process optimization methods.

CAMD tools utilize a database containing a few chemical groups that are used to generate and search a vast number of conventional or novel molecular structures to identify those molecules that offer the best performance with respect to the properties of interest [13]. This tool has been widely used in process and chemical industries. However its application to ORC has been mainly restricted to few research papers [5], [13], [14], [15]. Even in the CAMD method, the process optimisation and the pre-selection of working fluid candidates are decoupled. Bardow et. al [16] proposed a new route towards CAMD and its application to ORC was demonstrated by Lampe et.al.[5].

The aim of this work, documented in this report, is to develop a software tool which simultaneously optimizes the energy conversion process and selects the optimum working fluid for a given heat source. This tool is based on a framework that uses a Continuous Molecular Targeting approach to CAMD (CoMT-CAMD) which allows for an integrated working fluid and system design [5, 16]. The steady-state process is simulated with an in-house program for thermodynamic analysis and optimization of energy conversion systems [8]. The system model includes a simple design model of a radial turbine by using non-dimensional parameters [17] and a pinch point analysis model for the heat exchangers. Given constrained operating conditions, the ORC system is optimized simultaneously with the molecular parameters defining the fluid equation of state, the PCP-SAFT thermodynamic model [18][19]. This thermodynamic model provides an accurate description of actual fluids. The optimization is done in a state-of-the-art suite [20]. The working fluid is selected by comparing the optimized molecular parameters to the ones of real fluids.

The procedure has been preliminarily tested using as an example the specifications of a waste heat recovery ORC turbogenerator for truck engines [21]. The choice of the working fluid is restricted to siloxanes in the scope of this thesis. Once a sufficiently detailed and accurate molecular model is available, the scope of the tool can be extended to other fluids with detailed component models.

1-3 Thesis Outline

Chapter 2 presents the background literature review on the CAMD and CoMT-CAMD methods. Possible candidates for working fluids have also been described. The chapter ends with a literature review on the application of ORC to automotive heat recovery.
Chapter 3 presents the design on the software framework based on the CoMT-CAMD. A description of the thermodynamic model has been presented. The ORC system modeled in Cycle-Tempo has been described. The chapter proceeds onto a description of the preliminary turbine design model which has been implemented into Cycle-Tempo and the optimization algorithm and its implementation into this tool. The chapter concludes with an illustration of software architecture and the relationship between each component of the tool.
The report proceeds onto **Chapter 4** in which the simulations performed are described and the results are presented and discussed. Conclusions are drawn and recommendations are presented in **Chapter 5**.

Chapter 2

Background

The following chapter presents a brief review on the design methods for molecules in particular the CAMD and the Continuous Molecular Targeting approach to CAMD (CoMT-CAMD), working fluid candidates and ORC turbogenerators for automotive heat recovery.

2-1 Computer Aided Molecular Design (CAMD)

In principle, computer aided molecular design is the inverse of property prediction based on group contribution methods. The design of molecules is based on a systematic combination of a number functional molecular groups to develop a molecule with certain chemical structure and of particular physical and chemical properties which are calculated using Group Contribution methods that utilize databases containing the registered contributions of each functional group comprising the developed molecule. This, in addition to knowledge- or optimization-based technologies for screening molecules with desired properties, constitute the CAMD method. Papadopoulos et. al. [13] employed CAMD to design ORC working fluids. Figure 2-1 illustrates the traditional CAMD approach for design of fluids. From Figure 2-1, it is clear that the constraints on property values are obtained from a process-design optimization and the components are generated in the molecular-design step. The final selection of the fluid is based on a process wide objective such as cost, energy efficiency, etc. In such a method, there exists a possibility of ignoring the ideal candidate during the molecular design step as there is no feedback on the actual performance of the process for the component generated. Thus it is essential to integrate the molecular design with the process design. Bardow et. al [16] in their work, introduced a novel approach towards CAMD which establishes this integration between fluid and process properties. The following section introduces the continuous-molecular targeting approach to CAMD.

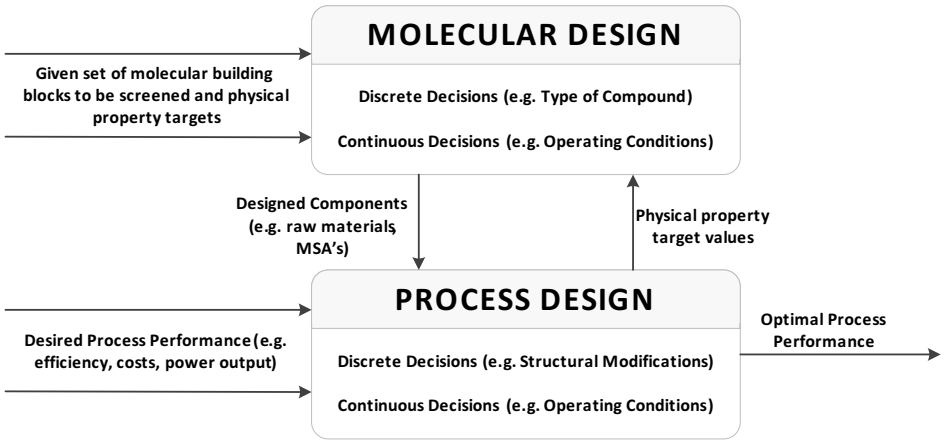

Figure 2-1: Traditional CAMD Approach (Adapted from Bardow et. al.[16])

2-2 Continuous-Molecular Targeting approach CAMD

While the idea to establish a link between process and fluid optimization seems quite straightforward [22], the actual implementation within a single mathematical optimization is prohibitive in most cases of practical interest due to a large amount of discrete variables. In practice, it is thus very difficult to simultaneously design working fluids and processes.

For the class of linear alkanes, Pereira et al. [23] pre-parameterized their thermodynamic model for this class of molecules to optimize the solvent chain length as part of process optimization. Unlike earlier thermodynamic models with lumped pure component parameters, recent developments have led to a physically based thermodynamic model in which a molecule is represented by a set of parameters which correspond to clearly defined molecular attributes.

The discrete parameters, in addition to the complex system design problem, present a mixed integer nonlinear programming (MINLP) problem, the solution to which is very difficult to realize in practical problems. Relaxation of the discrete model parameters representing the fluid circumvents the problem as it allows for a continuous search within the fluid parameter space. Optimization techniques can then be applied to simultaneously optimize the fluid and system. This is the first step of the Continuous Molecular Targeting approach. The result is a hypothetical target molecule for optimal system performance. In a second step, this molecule is mapped onto real fluid molecules [16].

Figure 2-2 illustrates the CoMT-CAMD problem formulation for working fluid selection. The following section presents the overview of the first step to the approach.

2-2-1 Step One: Continuous Molecular Targeting

The first step of the CoMT-CAMD aims to obtain the optimum settings for both the system and the molecular parameter set for a hypothetical working fluid from a simultaneous continuous optimization problem. The molecular parameters are relaxed in order to provide the opportunity for a continuous search in the full parameter set. The resulting optimization problem can be visualized as [16]

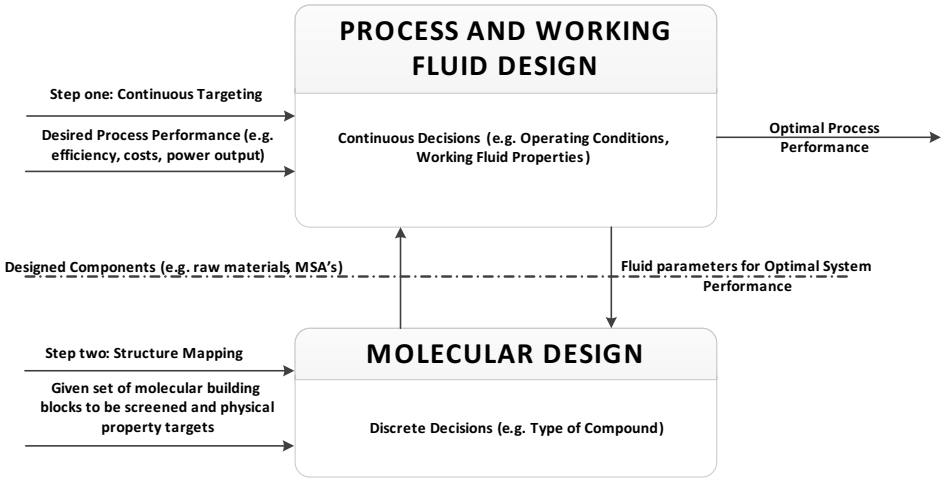

Figure 2-2: CoMT-CAMD problem formulation for integrated working fluid and system design (Adapted from Bardow et. al.[16])

$$max_{x,y} f(x) \tag{2-1}$$

$$s.t. \;\; h\left[x, \tilde{g}\right] = 0 \tag{2-2}$$

$$\tilde{g} - g(x, y) = 0 \tag{2-3}$$

$$c(x, y) \leq 0 \tag{2-4}$$

where x and y denote the process variables and the pure component fluid parameters respectively. **Equation** (2-1) refers to the design objective of the ORC system. The objective function can be either the efficiency of the complete system or the output power depending on the application. Commercially, ORC systems, as introduced in Chapter 1, are widely used as waste heat recovery systems in industries, conversion of geothermal heat, solar thermal systems for which fuel is not consumed directly and hence power output from the cycle becomes the main priority as the maximum efficiency point may not coincide with the maximum power point. In such cases, the objective function is defined as the power output. In ORC systems such as those used for biomass conversion, the objective function is defined as the net efficiency as the economic feasibility of such system depends directly on the fuel costs. In case of a multi-objective optimization problem, the total system cost can also be an objective for the optimization in which the solutions are those which do not dominate each other (also called non-dominated or Pareto-optimal solution). The selection of the final solution among optimum points located on the Pareto frontier requires a process of decision-making. In fact, this process is mostly carried out based on engineering experiences and importance of each objective for decision-maker [24].

Equation (2-2) represents the constraints applied to the system (x) and the fluid thermodynamic quantities ($\tilde{g}$). The thermodynamic properties of the fluid are computed from models $g(x, y)$ represented by (2-3). The process and fluid inequality constraints are summarized in (2-4).

To summarize, the essential elements of the first step are thermodynamic model, an ORC system model and an objective function. The following sections give a general background on each of these essential elements.

Thermodynamic Model: PCP-SAFT

Perturbed Chain Polar-Statistical Associating Fluid Theory (PCP-SAFT) equation of state (EOS) is a physically based equation which introduces a coarse-grained description of fluids, depicting molecules as chains of spherical segments [18][19][25][26]. The use of such a model enables the relaxation of the pure component parameters for the continuous molecular targeting step. The thermodynamic properties are derived from the residual Helmholtz free energy A_{res} as [27],

$$A_{res} = A_{hard-chain} + A_{dispersion} + A_{association} + A_{multipole} \tag{2-5}$$

The molecular model represented by the PCP-SAFT equation of state is illustrated in Figure 2-3. Each molecule is represented by a set of pure component parameters viz. [18]

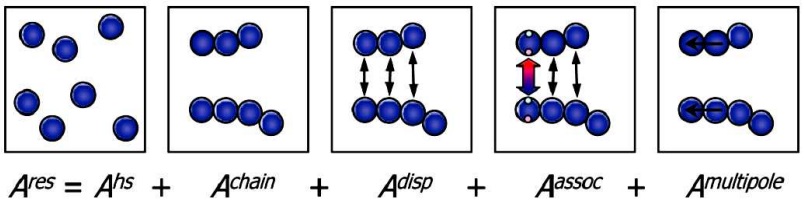

Figure 2-3: Residual Helmholtz energy and fluid interactions as described in the PCP-SAFT equation of state (adapted from Bardow et. al. [16])

- Geometric Parameters which describe the size and elongation, σ_i, m_i
- Energy-related parameters to describe the dispersive attraction, association energy and the association volume, ϵ_i/k, ϵ_i^{AB}/k, κ_i^{AB}
- Polar parameters that specify the point dipole and the quadrapole moments, μ_i, Q_i

The PCP-SAFT EOS provides a consistent description of all the residual thermodynamic properties of a molecule. The residual heat capacities, enthalpies, pressures and densities can be calculated from these pure component parameters. A detailed discussion of the implementation of the PCP-SAFT model has been done in Chapter 3.

System Model

The CoMT-CAMD framework is very flexible with the type of system to which it can be applied. The system is typically defined by its mass and energy balances in addition to the constrains on process variables such as maximum system pressure, condensing pressure, etc. The system model obtains thermodynamic input from the PCP-SAFT and the degree of freedom of the system serve as optimization variables in the continuous targeting step. The system model used in this work has been described in Chapter 3.

The next step of the approach is where discrete decisions have to be taken in order to map the fluid parameters from the optimization step onto real substances. The following section gives a brief background on the second step.

2-2-2 Step Two: Structure Mapping

The continuous molecular targeting step yields the optimum process setting with the optimal PCP-SAFT parameters of the hypothetical working fluid molecule. In order to translate these findings into reality, the fluid parameters have to be mapped onto real substances where discrete decisions have to be taken.

Group-contribution methods could be a suitable tool though they are still being developed for the most advanced SAFT models [16]. A database search to find the real molecule closest to the hypothetical solvent in parameter space seems to be an efficient method to find the real fluid. Bardow et. al [16] and Lampe et. al. [5] proposed the use of a Taylor approximation to predict the change in the objective function depending on the differences in the parameters given by

$$f(y) \simeq f(y^*) + \frac{\partial f}{\partial y}(y - y^*) + \frac{1}{2}(y - y^*)^T \frac{\partial^2 f}{\partial y^2}(y - y^*) \tag{2-6}$$

The mapping procedure implemented in this work has been described in Chapter 3.

2-3 Working Fluid Candidates

The important differences between water and organic fluid were highlighted in Chapter 1. The following section presents a brief review on potential working fluids. Working fluids may belong to the one of the following groups:

1. **Hydrocarbons**
2. **Perfluorocarbons**
3. **Siloxanes**
4. **Partially fluro-substituted straight chain hydrocarbons**
5. **Ether and fluorinated ether**
6. **Alcohols**
7. **Inorganics**

Table A-1 in Appendix A lists the potential working fluid candidates. Siloxanes are an interesting family of working fluids which have low- or non- toxicity, non-corrosiveness, good thermal stability and limited flammability, they are also good lubricants, and are used, as mixtures, as high-temperature heat transfer fluids [28]. Angelino and Invernizzi [29] studied the use of cyclic siloxanes in low-capacity space power cycles. They concluded that by adopting siloxanes as working fluids, a high overall conversion efficiency can be achieved by means

of a high degree of regeneration, moderate specific expansion work, low turbine rotational speed and significantly large volume flow rate at turbine outlet. Invernizzi et al. [30] studied exhaust gas heat recovery from small gas turbines by means of ORC systems in which cyclic siloxane D4 and linear siloxanes MM, MDM, and MD2M were considered as working fluids. Uusitalo et al. [28] evaluated the use of siloxanes as working fluid for a small capacity ORC turbogenerator based on the "high-speed technology" concept combining the turbine, pump and the generator on one shaft and the whole assembly is hermetically sealed and the bearings are lubricated by the working fluid. They concluded that the high molecular weight of siloxanes is beneficial in low power capacity (≈ 10 kW$_e$) applications because it leads to larger turbines with larger blade heights at the turbine rotor outlet and lower rotational speed when compared to toluene.

The scope of the current work is limited to the family of siloxanes which consists of cyclic fluids like Octamethylcyclotetrasiloxane, $C_8H_{24}O_4Si_4$ (D4), Decamethylcyclopentasiloxane, $C_{10}H_{30}O_5Si_5$ (D5), Dodecamethylcyclohexasiloxane,$C_{12}H_{36}Si_6O_6$ (D6) and linear fluids such as Hexamethyldisiloxane, $C_6H_{18}OSi_2$ (MM), Octamethyltrisiloxane, $C_8H_{24}Si_3O_2$ (MDM), Decamethyltetrasiloxane, $C_{10}H_{30}Si_4O_3$ (MD2M), Dodecamethylpentasiloxane, $C_{12}H_{36}Si_5O_4$ (MD3M) and Tetradecamethylhexasiloxane, $C_{14}H_{42}O_5Si_6$ (MD4M). The details of the limitation of the scope has been presented in Chapter 3. The following section presents one of the potential applications of ORC technology which has been used in this work.

2-4 ORC for Automotive Heat Recovery

The development of internal combustion engines has arguably saturated. However, these engines discharge approximately 66% of the fuel energy content as thermal energy to the environment [21]. It is therefore apparent that there exists a large untapped fraction of the primary energy which can potentially increase the overall efficiency by effectively recovering thermal power. ORC for heat recovery has already been widely exploited in stationary power plants as highlighted in Chapter 1. However the implementation on board of vehicles is challenging and no commercial application exists yet. A heat recovery system for an automotive engine must be efficient, small, lightweight, capable of highly dynamic operation, and satisfy the strict requirements of the automotive industry [21].

Investigation into the application of ORC for automotive heat recovery dates back to the 1970's in the United States as a consequence of the first oil crisis [31, 32, 33, 34]. An ORC system powered by the thermal energy of the exhaust of a 210 kW Mack ENDT 676 diesel truck engine was one of the first design and experimental studies. The working fluid was Fluorinol-50, an equimolar mixture of trifluoroethanol and water and a three stage axial turbine was designed, realized and tested successfully. The turbine was connected to a gear box with twice the rotational speed than that of the diesel engine. The measured conversion efficiency at maximum power output was 61.5% and ran for more than 78 hours of continuous operation [21, 31]. In a successive study [32, 33], a fluid with high thermal stability RC-1 was considered for an advanced supercritical regenerated cycle. A 15 to 18% fuel saving at cruising speed was estimated depending on the condensing temperature. A turbine diameter of 8.9 cm with a rotational speed of 55,000 rpm was a result of the preliminary design.

After a long absence, renewed interest into heat recovery is testified by several new research and development activities [21]. In a two-part article Teng et al. [35, 36] theoretically ana-

lyzed advanced heat recovery solutions for heavy-duty truck engines based on a supercritical reciprocating Rankine engine with pure and mixtures as working fluids. The authors report a conversion of about 20% of the total energy discharged by the diesel engine to mechanical power.

Lang et al. [21] documented a feasibility study and performance evaluation of an ORC turbogenerator as the high temperature heat recovery system employing a siloxane as the working fluid. A high speed turbine was selected as the expander due to its advantages such as smaller dimensions, no need of internal lubrication, higher efficiency and lower maintenance over competing technologies such as piston expanders and scroll expanders. This work has been used as a reference to validate the model developed within the scope of this thesis.

Chapter 3

Model

The following chapter describes the design procedure of the software tool based on the CoMT-CAMD approach to simultaneously optimize the working fluid and system for an ORC turbogenerators in automotive heat recovery introduced in Chapter 2. An outline of each step of the CoMT-CAMD method was presented in the previous chapter. The design and its implementation have been outlined in this chapter. The chapter then proceeds onto the software framework illustrating the architecture of the tool and the relationships between each software.

3-1 Thermodynamic Model

The PCP-SAFT EOS presents a coarse-grained description for a fluid. The family of siloxanes have been considered as candidates for working fluids for its properties stated earlier in Chapter 2. In addition to its properties, this limitation is imposed as the objective of the current work is to translate the CoMT-CAMD method into an automated working tool with the important elements such as preliminary turbine model, heat exchanger pinch point, etc. Table 3-1 lists the molecular parameters of the PCP-SAFT EOS for siloxanes.

Table 3-1: Molecular parameters of the PCP-SAFT EOS for siloxanes [37]

Fluid Short Name	Molecular Mass [kg/k-mol]	Accentric Factor [-]	Segment Number [-]	Segment Diameter [Å]	Segment Energy [K]
D4	296.616	0.589	5.754	4.124	213.874
D5	370.769	0.666	6.303	4.324	217.780
D6	444.924	0.746	7.017	4.444	220.355
MM	162.379	0.419	4.243	3.979	209.493
MDM	236.530	0.531	5.150	4.169	213.382
MD2M	310.690	0.589	6.196	4.246	212.600
MD3M	384.843	0.741	6.954	4.260	215.338
MD4M	459.000	0.821	7.482	4.511	219.148

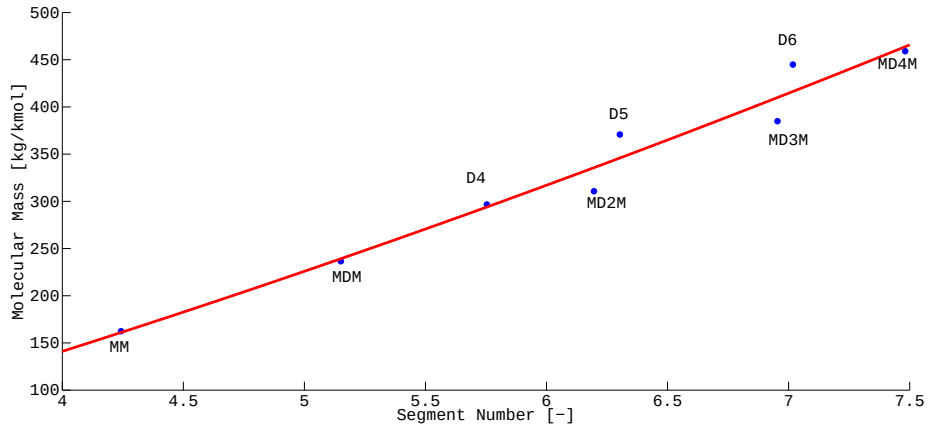

(a) Molecular mass

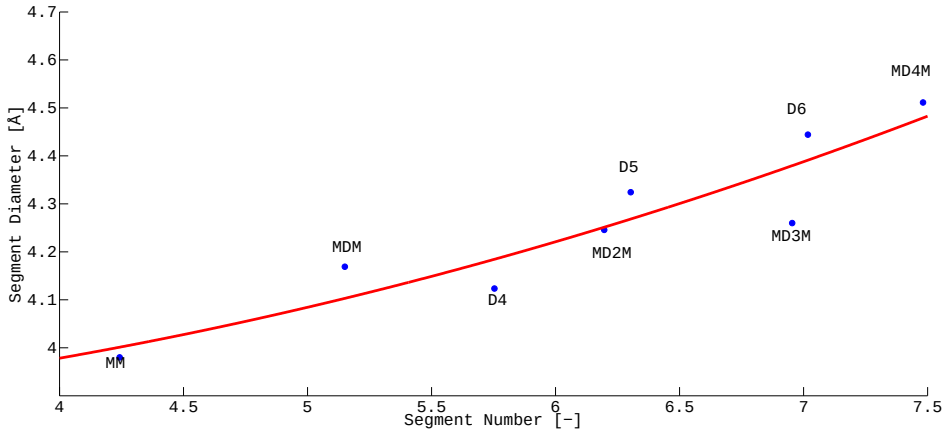

(b) Segment Diameter

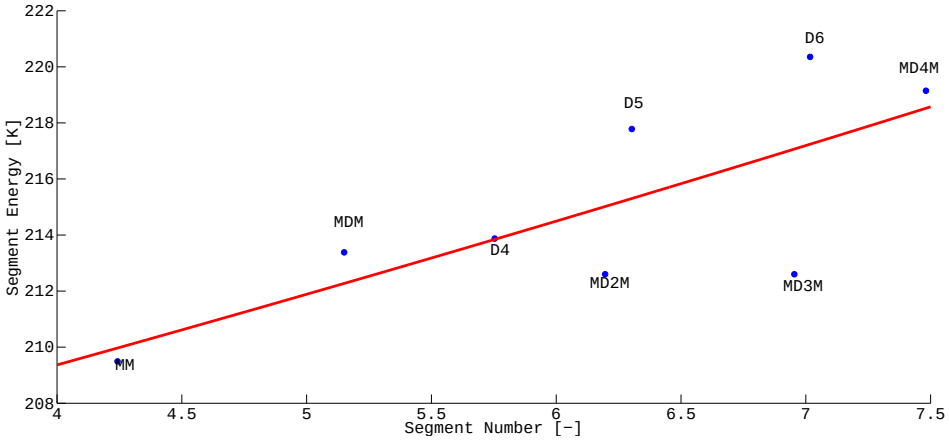

(c) Segment Energy Parameter

Figure 3-1: Molecular mass and Pure component parameters as a function of segment number

Lampe et. al. [5] have considered the pure component parameters (m, σ_i, ϵ_i/k) as variables for the optimization problem. However, as a first step towards developing this tool, the segment number (m) has been considered as the only optimization variable for the fluid and the other parameters are represented as polynomial functions of the segment number illustrated in Figure 3-1(a), Figure 3-1(b) and Figure 3-1(c). Mixtures of siloxanes and polar contributions have not been considered in this work but they can be readily integrated in the future.

Table 3-2: Coefficents for ideal gas specific heat capacity based on equation (3-1) [37]

Fluid Short Name	A [J/mol-K]	B 10^3[J/mol-K^2]	C 10^6[J/mol-K^3]	D 10^9[J/mol-K^4]
D4	84.936	1086.740	-512.950	22.309
D5	90.971	1564.410	-1091.370	340.089
D6	134.789	1738.840	-1049.940	256.444
MM	51.894	741.340	-416.100	70.000
MDM	-6.164	1184.230	-679.873	145.228
MD2M	-10.805	1532.360	-889.822	192.240
MD3M	-15.425	1880.400	-1110.060	239.210
MD4M	-20.071	2228.540	-1311.430	286.228

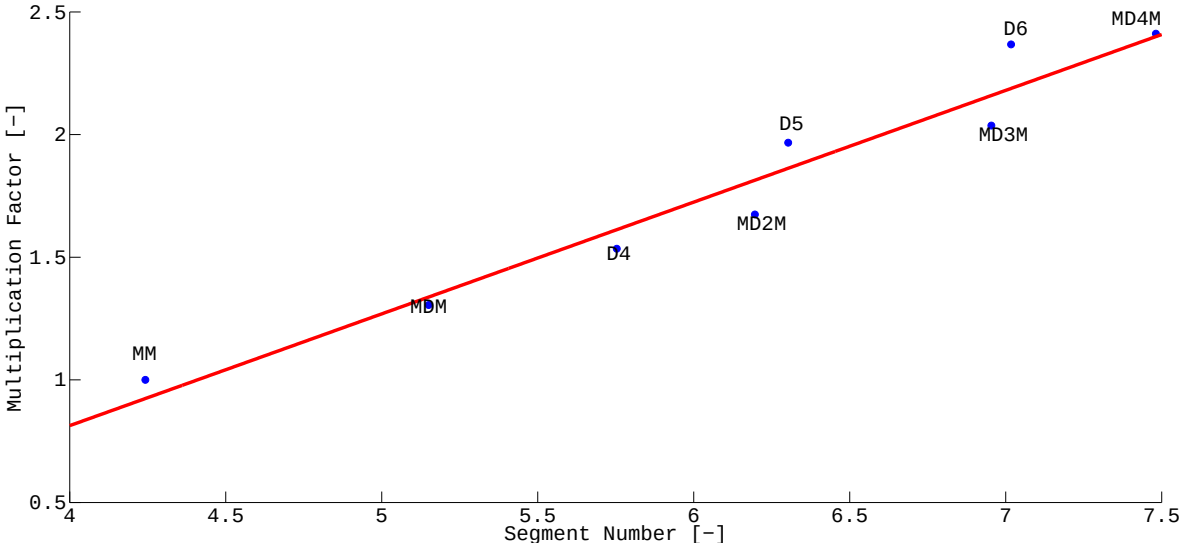

Figure 3-2: Linear fit of the multiplication factor for each siloxane

In order to calculate the output power and enthalpies for a hypothetical fluid, it is essential to define the coefficients of the ideal gas heat capacity. Table 3-2 lists the coefficients for the ideal gas heat capacity which is based on the following equation:

$$C_p = A + BT + CT^2 + DT^3 \tag{3-1}$$

where T is the temperature (in K). In the absence of a model to predict the ideal gas heat capacity of the hypothetical fluid from PCP-SAFT parameters, a representative polynomial function has been derived. MM is the most basic fluid in the siloxane family as it has the smallest segment number as seen in Table 3-1. A multiplication factor has been defined for each fluid which is an average of the ratio of the Cp of each fluid and Cp of MM at the

corresponding temperatures given by (3-2)

$$Multiplication\ Factor, MF = \frac{C_{pSiloxane}(T)}{C_{pMM}(T)}, \qquad 80 < T(^oC) < 400 \tag{3-2}$$

The multiplication factor for each fluid was plotted against the corresponding segment number and fitted to a line as illustrated in Figure 3-2. The linear fit is represented by the equation,

$$MF = 0.4556 * m - 1.0091 \tag{3-3}$$

Thus, the coefficients of the ideal gas heat capacity are represented by equations (3-4)-(3-7)

$$A_{Fluid} = MF * A_{MM} \quad [J/mol - K] \tag{3-4}$$
$$B_{Fluid} = MF * B_{MM} \quad [J/mol - K^2] \tag{3-5}$$
$$C_{Fluid} = MF * C_{MM} \quad [J/mol - K^3] \tag{3-6}$$
$$D_{Fluid} = MF * D_{MM} \quad [J/mol - K^4] \tag{3-7}$$

The calculated coefficients for the fluid are then used to determine the Cp at the corresponding temperature using equation (3-1). The equations derived from the fitting of the parameters to the segment number are listed in Appendix B

Now that the important parameters of the PCP-SAFT have been represented in terms of a single variable, it is essential to define a system model. The following section provides a detailed description of the ORC turbogenerator system introduced previously in Chapter 2.

3-2 System Model

An ORC system to recover waste heat from a truck has been considered for this work. Figure 3-3 illustrates a typical energy flow in a diesel engine of a truck. In such engines, high-grade thermal energy can not only be efficiently recovered from the exhaust but also from the exhaust gas recirculation (EGR) system. The heat recovery system has been designed at average cruising speed and load for the considered heavy-duty truck engine; therefore at 50% of the maximum power at 1500 rpm. Due to considerations concerning the control of the system, a configuration with two parallel high temperature evaporators has been chosen [21]. A three-way controlled valve is needed to regulate the working fluid flow. Other sources of heat such as the coolant and charge air coolers are not feasible sources of heat as this would require a high working fluid flow rate which would lead to large evaporator and condenser in addition to a low waste heat recovery efficiency [36] and hence not feasible for on-road vehicle applications.

The coolant for the engine is assumed to be pure water. The flue gas composition is based on the exhaust data for a diesel engine given by Bombarda et. al [38] which has been listed in Table 3-4. The values for the mass flow, temperature, and pressure of the gases in the exhaust

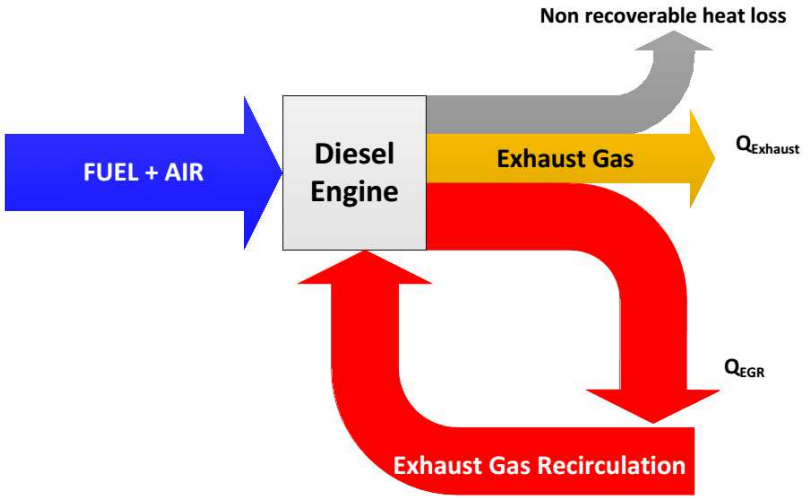

Figure 3-3: An illustration of the Sankey diagram of a diesel engine (Energy flow not to scale)

and in the EGR system are taken from accurately measured engine maps [21] and have been reported in Table 3-3. Pressure drops of 5kPa and 0.5kPa are assumed in the working fluid side and flue gas side of the heat exchangers respectively based on the heuristic knowledge that plate type heat exchangers have low pressure drops.

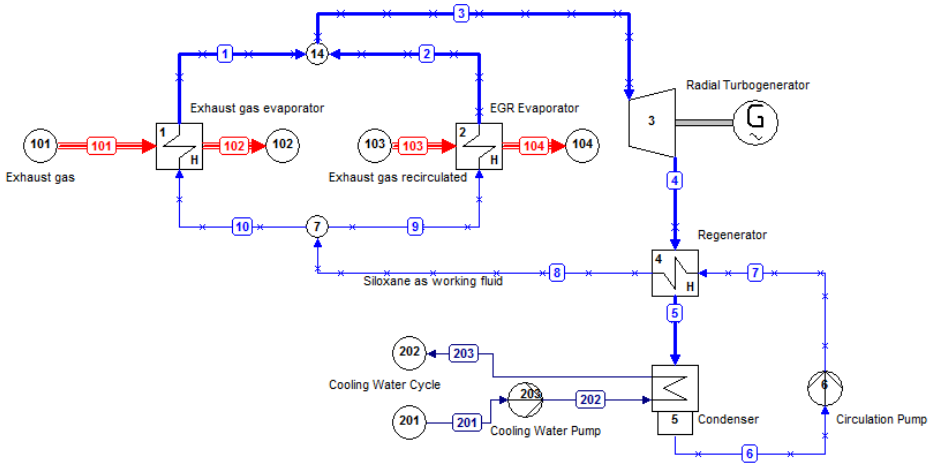

Figure 3-4: System Layout of ORC turbogenerator for automotive heat recovery [8]

A 5 K of superheating with respect to the temperature at the corresponding evaporation pressure has been specified to ensure that no liquid droplet can enter the turbine [21]. A high speed turbine has been implemented because of its advantages over piston and scroll expanders described previously in section 2-4, the details of which are described in the following sections. A regenerator is used to recover heat from the vapor leaving the turbine to preheat the fluid entering the evaporator. Constraints on the heat exchanger pinch point have been considered which are discussed later in section 3-4. The condenser is also bound by the cooling water flow rate in addition to the volumetric flow rate from the turbine outlet. The amount of head available for the cooling water circulation pump in a truck is limited. Hence, this pump has

Table 3-3: Main characteristics of the ORC system

Parameter	Unit	Value
Gas mass flow rate - Exhaust	kg/s	0.225
Gas mass flow rate - EGR	kg/s	0.127
Gas temperature - Exhaust evaporator inlet	^oC	307
Gas temperature - EGR evaporator inlet	^oC	429
Circulation Pump Isentropic Efficiency	%	65
Cooling Water Pump Isentropic Efficiency	%	75
Superheating at turbine inlet	K	$T_{evap} + 5$
Maximum evaporation pressure	bar	40
ΔT pinch point regenerator	K	25
ΔT pinch point condenser	K	5
Mechanical efficiencies (pump, turbine)	%	98
Lower terminal temperature difference in evaporators	K	25

Table 3-4: Flue gas composition based on Bombarda et al. [38]

Component	Percentage [%]
Nitrogen	74.6
Oxygen	11.7
Steam	6.7
Carbon dioxide	5.9
Argon	1.1

been considered to be part of the auxiliary power consumption to limit the cooling water flow rate and allow for a realistic condenser. The isentropic efficiency of the pumps have been specified based on heuristic knowledge from similar systems.

Figure 3-4 illustrates the process flow diagram of the ORC system described above which has been modeled in Cycle-Tempo [8]. One of the most critical component of this system is the turbine; therefore its feasibility has been evaluated by performing the preliminary design of a radial turbine. The following section presents a description of this model.

3-3 Turbine Model

Organic fluids exhibit significant advantages in a variety of applications; one of the most important being the possibility of designing low stress, economic and efficient turbines for temperature ranges at which a steam turbine becomes unattractive and inefficient [39]. These fluids possess certain characteristics which influence the design of turbines. These are:

1. **Small Enthalpy Drop**

   Enthalpy drop is relatively small due to the fluid's large molecular mass. Thus there exists a possibility for designing a single-stage high-velocity ratio turbines with moderate peripheral speed and centrifugal stresses.

2. **Low speed of sound**

   The low speed of sound results in high Mach numbers of inlet flow velocity relative to the rotor velocity. This influences the design of the rotor inlet and outlet as the Mach numbers should be limited to minimize shock losses.

3. **Large expansion Ratio**

   It implies a larger volume flow rate ratio per stage and hence presents difficulties in the form of large rotor blade height variation between the inlet and outlet and higher Mach numbers.

4. **Higher density and lower specific volume**

   These properties allow the use of a turbine with smaller overall dimensions and flow passage when compared to water.

Thus some compromise must be found between the volume flow ratio and enthalpy drops to allow reasonable inlet Mach numbers and rotor blade height variations. A single stage axial turbine can be used if the volume flow ratio is not too high. In case of high volume flow ratio, multi-stage axial flow turbine or radial(centrifugal) flow turbines can be considered.

The thermodynamic system considered, in this work, requires the turbine to be small and light because of the type of application. An axial turbine is a less attractive option because the blades have to be made very small and numerous which leads to higher friction losses and blockage effects. Furthermore, the running clearance necessary between blade tips and shroud become a significant fraction of the blade height and thus the tip leakage losses can be quite severe. Another disadvantage of a small axial turbine is the increase in problems and expenses of manufacturing of the blades. Sauret and Rowlands [40] mention a few advantages of using a radial turbine for ORC systems such as better off design performance, less sensitivity to blade profile inaccuracies, robustness under increased blade load and relative ease of manufacturing. Thus considering the limitations on the dimensions and weight, a radial turbine has been considered. The following sections outline the details of a radial turbine model used in this work.

3-3-1 Radial Turbine

A Radial turbine is a work producing device which consists of essentially two parts: a stator in which the working fluid is expanded and turned to give it a circumferential velocity about the axis of the machines and a rotor through which the flow passes and produces work. Additionally, an inlet is provided to guide the fluid to the stator. Downstream of the rotor, the fluid often has significant velocity and hence by means of employing a diffuser can be recovered. The following paragraphs highlight the important parts of a radial turbine [1].

Inlet

Working fluid most commonly approaches either in an axisymmetric annular flow or in the tangential direction. In the former case, the flow enters the stator in a radially inward direction and the vanes must turn it to give it swirl or tangential velocity at the inlet to the rotor. In the latter case, the design of the inlet casing must be such as to turn the linear approaching flow and distribute it about the circumference of the turbine and hence the casing is made in a spiral shape with maximum cross-section area at inlet and decreases with azimuth angle about the turbine axis. This casing is often called a volute or scroll.

In this work, the flow is considered to be entering in an axisymmetric annular direction and hence a vaned nozzle is required at the inlet in order to provide the swirl component to the velocity. Figure 3-5 illustrates a radial turbine with vaned nozzle.

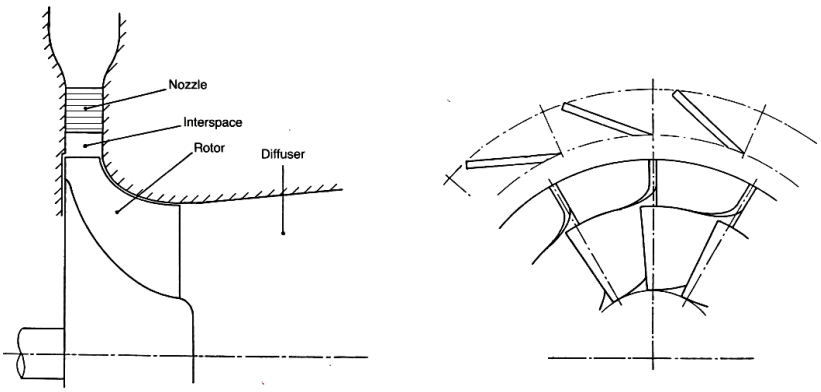

Figure 3-5: Radial Turbine with vaned nozzle (adapted from Whitfield and Baines [1])

Stator

The fluid enters in a radially inward direction where in the fluid must be turned by an annular ring of vanes in order to give it a swirl or tangential velocity and accelerated before entering the rotor. These vanes are required to perform a similar role as the nozzle guide vane row of an axial turbine and is often developed from an axial section geometrically transformed into the radial plane. A minimum working clearance must be left between the vane trailing edges and the rotor tip. In cases where the flow enters in a tangential direction, the stator is much simpler in design.

The stator has a large influence on the mass flow rate of the fluid in the turbine. At high pressure ratios, a nozzled turbine chokes at the throat and limits the mass flow rate. The stator losses are relatively smaller in magnitude when compared to the rotor losses and hence can be ignored in some cases. However the losses may be higher in case of a very high pressure ratio wherein supersonic expansion occurs downstream of the throat accompanied by turning of the flow towards the radial direction leading to shock waves. As this area is still not investigated completely, these losses have not been considered in this preliminary design.

Rotor

The purpose of the rotor is to transfer the kinetic energy of the moving fluid to the output shaft. Its design and performance is strongly influenced by the design of the stator. Furthermore, the rotor is a major source of loss generation through effects like skin friction on the rotating blades and hub and the stationary casing, over-tip leakage in the clearance gap between the blades and the casing and secondary flows which distributes a low momentum boundary layer fluid through the passage which are .

The flow at the inlet of the rotor is predominantly in a radial-tangential plane and in the inward radial direction. Work extraction proceeds very quickly as the flow moves inwards

due to which the radius and hence the blade speed and the tangential velocity of the vapor decrease. This implies a high cross-stream pressure gradient between the blades i.e. high blade loading.

The rotor contains an axial to radial turn in the meridional plane and at the same time, the blades must curve towards the exit. These two curvatures in addition to the effects of rotation of the passage about the turbine axis result in a very complex 3-D flow pattern. The meridional curvature sets up a secondary flow which tends to move the fluid from the hub to the shroud while a recirculation continues to move it from the pressure to suction surface.

In the exit section, the primary flow is on an axial-tangential surface of revolution about the axis and any radial components of velocity are small. The function of the exducer (or exit section) is to turn the flow from a predominantly axial direction in the relative frame and give it relative tangential momentum which is important in determining the level of work output from the rotor. Figure 3-6 illustrates a 3-D model of a radial turbine rotor.

Figure 3-6: An illustration of the rotor of a radial turbine [41]

Exhaust Diffuser

The working fluid leaving the rotor has certain kinetic energy which can be quite significant in cases where the size and weight of the machine are important and the rotor exit blade height is kept small. The energy is wasted unless the fluid can be diffused. A diffuser increases the expansion ratio across the rotor over a fixed pressure ratio. However there are certain drawbacks of having a diffuser. It adds considerably to the overall size of the turbine. Also, a sharp bend immediately after a diffuser imposes a pressure gradient across the stream which can seriously reduce its efficiency. Another problem is that the exhaust of a turbine in off-design performance is usually not axial but highly swirling. If this swirling is considerable, it is associated with a centrifugal pressure field which can cause the diffusion to break down and fluid to recirculate.

Based on the theory discussed above, a preliminary model of a radial turbine has been implemented. The following section describes this model.

3-3-2 Preliminary design of radial turbine

The application plays an important role in defining the turbine's performance in terms of quantities such as pressure ratio and required power output or flow rates and speed of rotation. Other requirements such as maximizing efficiency or specific work transfer (and hence minimizing size) also need to be considered which are often in conflict with the application based parameters mentioned earlier. Thus it is important to have the right balance between these two class of parameters. The objective and scope of this model is to correlate the turbine isentropic efficiency with the corresponding fluid properties and does not provide the final optimum dimensions of a turbine. Certain assumptions are made in this design procedure. These are listed in the following section.

Assumptions

The model is based on the procedure which uses non-dimensional parameters. The assumptions and scope of this model are:

1. The methodology is commonly used for incompressible flow machines but can be extended to compressible flow machines [1].
2. The flow in the rotor is extremely complicated with unsteady, 3-D, viscous and compressible flows with complicated secondary flows. The preliminary design is a very simplified representation of the real flow.
3. The design process is more concerned with the aerodynamic considerations without any mechanical stress analysis except in conditions where the knowledge of experience can be used.
4. The stator (nozzle) geometry has not been considered.
5. Due to the comparatively large expansion ratio resulting from the thermodynamic cycle design, the absolute velocities at the nozzle outlet are supersonic. This results in an uncertainty over the predicted turbine performance, because there are no validations available for organic fluids with supersonic rotor inflow conditions.
6. Because of the strict constraints on sizes, an efficient diffuser cannot be designed; thus its possibly beneficial effect is also neglected.
7. The loss coefficients for the nozzle and rotor have been assumed based on practical values available for well-designed nozzle and rotor for 90^o inflow radial turbines [17].
8. The method uses some empirical values which are not available for the high-expansion ratio typical of high-temperature ORC turbines. These values were therefore assumed, resulting in a certain degree of uncertainty on the predicted isentropic efficiency [21].

Based on these assumptions, a model has been implemented which is discussed in the following section.

Turbine Model Implementation

The radial turbine has been modeled in FORTRAN and implemented into Cycle-Tempo. The input to the procedure are the system specifications such as mass flow-rate, turbine inlet temperature, fluid velocity and non-dimensional design parameters such as degree of reaction, flow coefficient and spouting velocity ratio. The outputs are the basic dimensions of the inlet and exit planes of the rotor in terms of diameter, blade height and angle and the power output, isentropic efficiency and speed of rotation. The non-dimensional parameters are expressed as:

$$R = \frac{h_2 - h_3}{h_1 - h_3} \tag{3-8}$$

$$\phi = \frac{C_{m3}}{U_2} \tag{3-9}$$

$$\psi = \frac{U_2}{C_o} \tag{3-10}$$

where R is the degree of reaction, h_x is the static enthalpy at station x, C_{m3} is the absolute velocity of fluid flow in the meridonal direction at station 3, U_2 is the rotor tip speed, C_o is the isentropic spouting velocity at the turbine exit which would result in an ideal expansion of the gas over the same pressure ratio as that of the turbine. The parameters ϕ and ψ are analogous to the flow and blade loading coefficients used in axial turbines [1]. Figure 3-7 presents the relationship between these parameters [42].

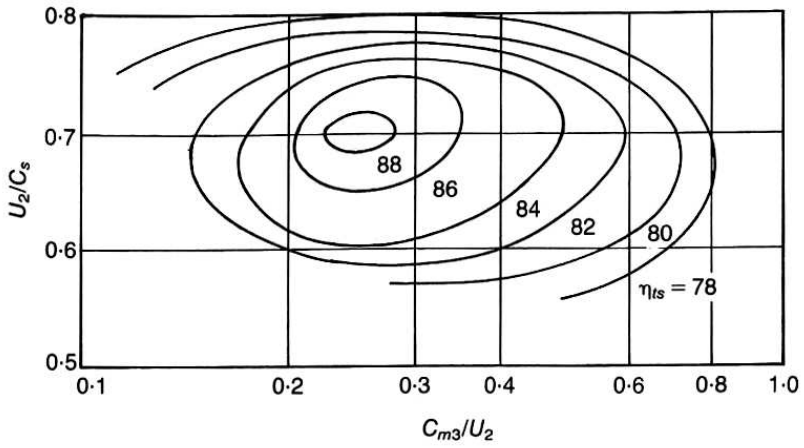

Figure 3-7: Correlation of attainable radial turbine efficiencies with velocity ratios (from Rodgers and Geiser [42])

From the figure, it is clear that the maximum efficiency is achieved when the values of ϕ and ψ are 0.25 and 0.7 respectively. The degree of reaction is typically between 0 to 0.5 [43]. In conventional impulse stages (R=0), supersonic relative inlet velocity is obtained for volume ratios larger than 5 while for a 50% reaction stage, subsonic rotor inlet conditions are achieved for volume ratio of about 500 but the rotor blade height variations are prohibitive

and infeasible [39]. A low degree of reaction reduces the pressure drop in the rotor and limits sealing problems in addition to achieving expansion in a single stage[17, 44]. Hence, a reaction of about 0.15 has been chosen in this work. A well designed nozzle, in general, has a high isentropic efficiency and hence a value of 95% has been considered. The blades are assumed to be radial at the inlet to reduce bending stresses [17]. The parameters associated with the inlet velocity triangle have to be calculated as it is important to compute the Mach number which is required for the preceding nozzle design. Although the inlet Mach numbers can be in excess of the minimum, it is essential to limit its value as higher values lead to increased stator losses, higher velocities in the rotor and increased incidence losses.

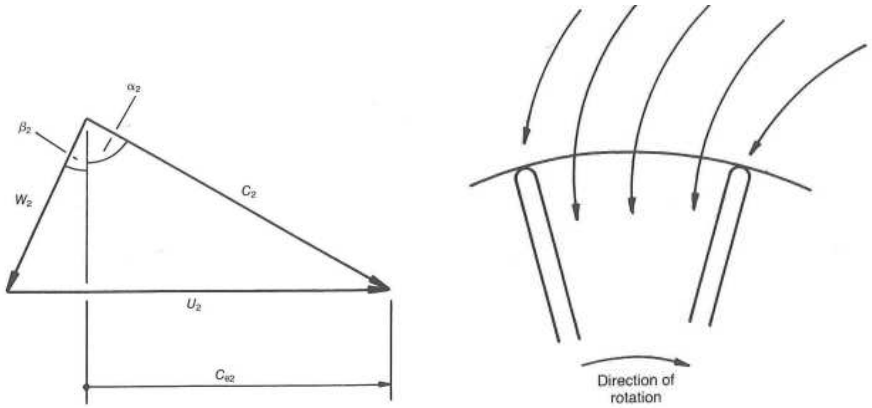

(a) Velocity Triangle (b) Rotor Inlet Flow

Figure 3-8: Rotor inlet flow and velocity triangle (from Whitfield and Baines [1])

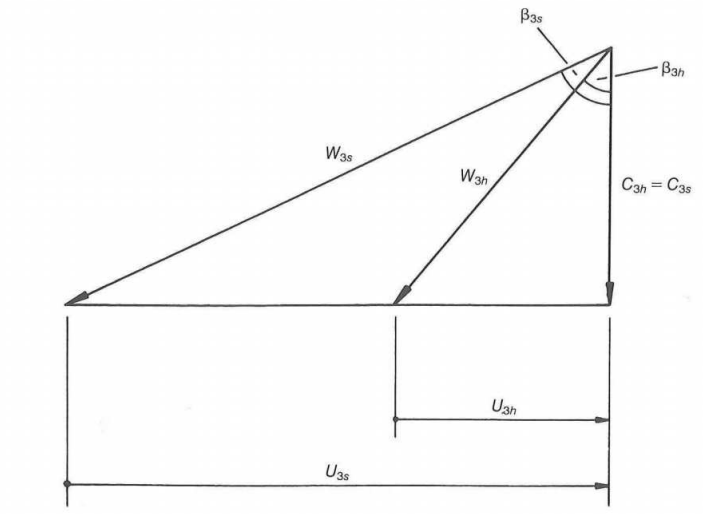

Figure 3-9: Velocity triangles at rotor exit hub and shroud (from Whitfield and Baines [1])

For the rotor exducer, a similar analysis is applied. The exit of the rotor is assumed to have no swirl velocity. The exit velocity can be determined by using the exit velocity ratio ϕ. The rotor exit geometry is determined by the exit hub to shroud diameter ratio D_{3h}/D_{3s} and the diameter ratio D_2/D_{3rms}. Rohlik [45] suggested that the exit hub to shroud diameter

ratio D_{3h}/D_{3s} should be greater than 0.4 in order to reduce the secondary flow and avoid flow blockage caused by closely spaced vanes. Hence the minimum value of 0.4 has been considered. The diameter ratio D_{3s}/D_2 should not be more than 0.7 in order to avoid excessive shroud curvature [45]. This ratio is assumed to be 0.5. The turbine exit velocity is assumed to be 60 m/s [28]. Table 3-5 summarizes the important parameters discussed above. The details of the calculation procedure has been described in appendix B.

Table 3-5: Input parameters for the model[1][43]

Parameter	Value
Degree of Reaction, R [-]	0.15
Exit Velocity Ratio, ϕ [-]	0.25
Spouting Velocity Ratio, ψ [-]	0.7
Isentropic Efficiency of Nozzle, η_{nozzle}[%]	0.95
Inlet Velocity, c_1 [m/s]	0
Exit Velocity, c_4 [m/s]	60
Exit hub to shroud diameter ratio, D_{3h}/D_{3s} [-]	0.4
Diameter ratio, D_{3s}/D_2 [-]	0.5
Solidity, [-]	6

Efficiency calculation

The final step in the turbine model is to compute the isentropic efficiency using the calculated values of fluid properties, angles and dimensions. The performance of turbomachines can be easily evaluated by using $n_s d_s$ diagram [46] as shown in Figure 3-10.

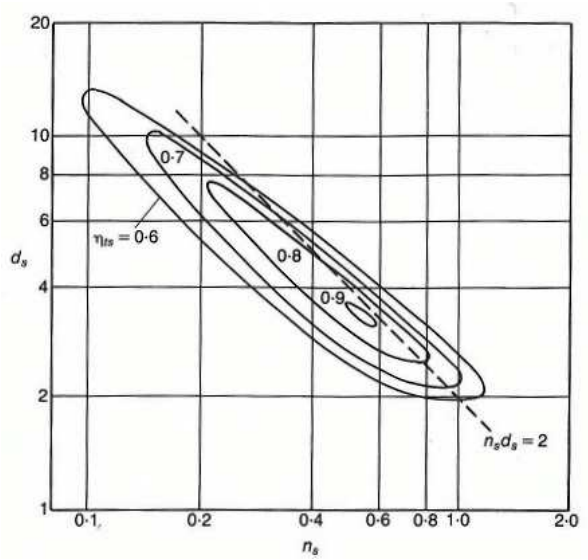

Figure 3-10: $n_s d_s$ diagram (from Balje [46])

The $n_s d_s$ diagram does not include the losses in the nozzle and rotor. In addition, the need to integrate the model into a continuous procedure makes it difficult to use this chart. Dixon [17] presents an expression for nominal isentropic efficiency in the absence of a diffuser

which is defined as

$$\eta_{ts} = \frac{h_{01} - h_{03}}{h_{01} - h_{3ss}} = \frac{\Delta W}{\Delta W + \frac{1}{2}c_3^2 + (h_3 - h_{3s}) + (h_{3s} - h_{3ss})} \tag{3-11}$$

where h_{0x} is the stagnation enthalpy at station x, h_{3ss} is the point of complete isentropic expansion shown in Figure 3-11, ΔW is the specific work of the turbine, c_3 is the absolute velocity of fluid flow.

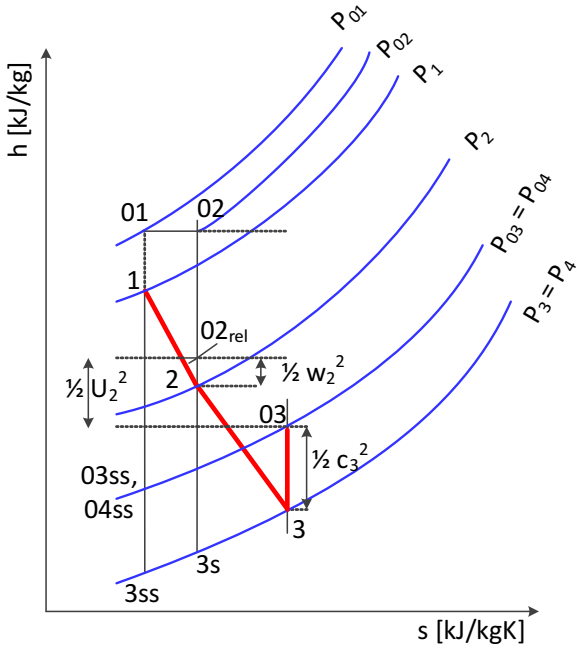

Figure 3-11: h-s diagram of the radial turbine expansion

The passage enthalpy losses can be expressed as a fraction of the exit kinetic energy relative to the nozzle row and the rotor, i.e.,

$$\begin{aligned} h_3 - h_{3s} &= \frac{1}{2}w_3^2\zeta_R \\ h_{3s} - h_{3ss} &= \frac{1}{2}c_2^2\zeta_N(T_3/T_2) \end{aligned} \tag{3-12}$$

where ζ_R and ζ_N are loss coefficients at the rotor and nozzle respectively, w_3 is the relative velocity of fluid flow, c_2 is the absolute velocity of fluid flow, T_x is the static temperature at station x. Using (3-12) in (3-11) we get,

$$\eta_{ts} = \left[1 + \frac{1}{2}(c_3^2 + w_3^2\zeta_R + c_2^2\zeta_N T_3/T_2)/\Delta W\right]^{-1} \tag{3-13}$$

The nozzle and rotor loss coefficients are assumed to be 0.1 and 1.0 respectively based on the range of practical values for well-designed nozzles and rotors given by Dixon [17]. Equation (3-13) is valid for nominal design point calculations(incidence-free operation). The validity can be extended to off-design operation by including an incidence loss coefficient while evaluating the velocity coefficient in the rotor [46]. Benson [47] presents a review of the method to

evaluate this incidence loss for radial gas turbines. However, due to lack of literature available on the evaluation of incidence loss for organic fluids, the nominal design point efficiency has been considered to be the isentropic efficiency.

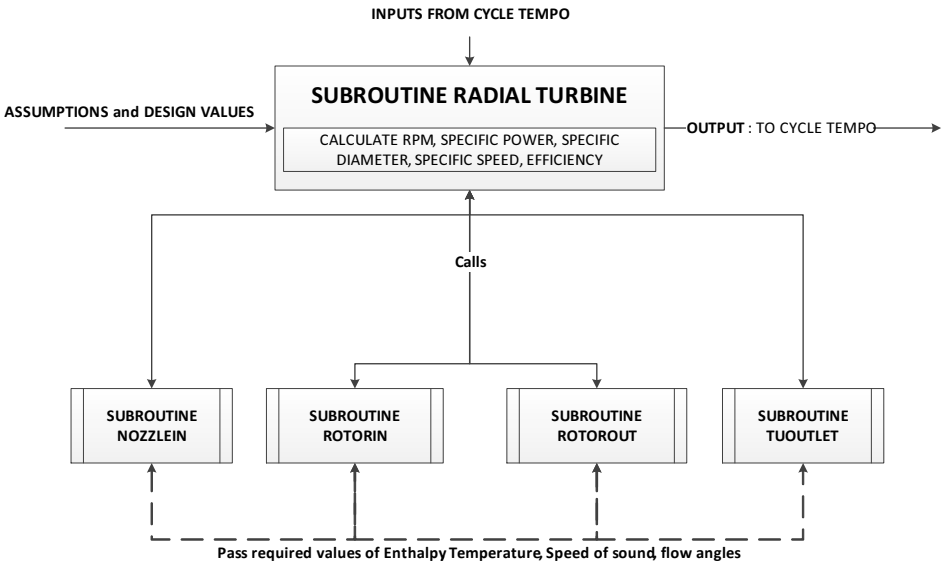

Figure 3-12: Architecture of the Radial Turbine Model implemented in Fortran

Figure 3-12 illustrates the architecture of the radial turbine model discussed above. The model can be chosen by a unique identification code in Cycle-Tempo. The input values of the cycle are provided from Cycle-Tempo into the main subroutine. The assumptions and design values are also input to this subroutine. Each station of the turbine has been implemented in a different subroutine and these interact by passing the required parameters to each other. The details of the calculation procedure and the individual subroutines can be found in appendix B.

3-4 Pinch Point Calculation

The most critical components apart from the turbine are the heat exchangers. Although a detailed heat exchanger design is out of the scope of this work, it is however essential to make sure that the heat exchangers operate in accordance with the second law of thermodynamics. Hence a pinch point analysis of the heat exchangers present in the system has been done The pinch point is defined as the point at which the temperature difference between the hot and the cold fluid is minimum.

The system has four heat exchanging equipments which need to comply to the second law of thermodynamics. The pinch points in the regenerator and the condenser are defined by their terminal temperature differences which are given as inputs to the system model. However, in case of the evaporator, the pinch point can be either at the lower temperature terminal or at the saturated temperature (in sub-critical cycles) or at point where the slope of the curves are equal (in supercritical cases). Figure 3-13(a) and Figure 3-13(b) illustrate typical T-Q diagrams for the evaporator in subcritical and supercritical cycles respectively.

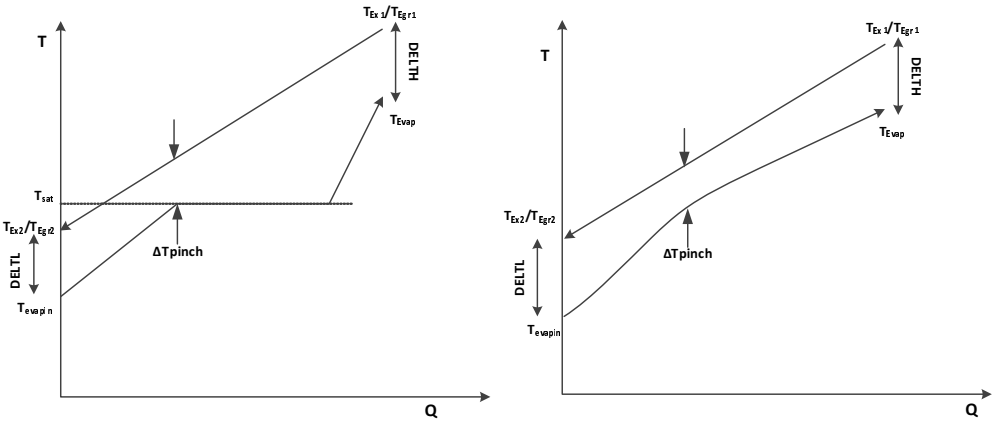

(a) Sub-critical conditions (b) Super-critical conditions

Figure 3-13: Evaporator T-Q diagrams

A function to calculate the pinch point temperature difference for the evaporators has been implemented to prevent the violation of the second law of thermodynamics. For supercritical conditions, the T-Q diagram is divided into a number of small subsections and the temperature difference at each section is calculated. The minimum temperature difference gives the approximate location of the pinch point. For sub-critical conditions, an energy balance is done in the evaporator. The temperature difference between the saturated temperature and fluegas temperature is evaluated. The minimum value of either the lower terminal temperature difference or this difference is the location of the pinch point. Appendix B lists the MATLAB function for pinch point evaluation implemented in this work. In order to define an optimization problem, it is important to define its objective. The following section describes the definition of this objective function.

3-5 Objective Function

The objective function can include not only the working fluid properties but also system objective functions. Thus by combining both of them, a trade-off between different working fluids and its effect on the system is directly achieved. A number of properties based on Thermodynamic, Environmental, Safety and System-related performance measures as proposed in the work of Papadopoulos et al. [13] can be considered in order to find the potential working fluid candidates. These properties are elaborated as follows:

1. *Density* (ρ) of the working fluid should be high either in liquid or vapor phase as it leads to increased mass flow rate and reduced equipment size.

2. *Latent heat of vaporization* (H_v) of the working fluid may be high as it enables most of the available heat to be added during the phase change operation and hence in this process, avoiding the need to regulate super-heating [48]. However, according to Yamamoto T. et al. [49], as the Turbine Inlet Temperature cannot be controlled for low grade heat sources, the working fluid must have low latent heat in addition to high density to increase the turbine inlet temperature. These contrasting arguments need to

be evaluated further and hence the latent heat of vaporization is not considered as a fluid performance measure in this work.

3. *Viscosity* (μ) of the working fluid should be low in both liquid and vapor phases in order to increase the heat transfer coefficient with reduced power consumption.

4. *Thermal Conductivity* (λ) must be high to have a high heat transfer coefficient in the heat-exchangers.

5. *Ozone Depletion Potential* (ODP) and *Global Warming Potential* (GWP) should be either very low or zero. ODP can be calculated by using correlations and data available in literature. Calm et. al. [50] have proposed generic guidelines for estimation of ODP and GWP for refrigerants. Kazakov et. al. [51] have recently developed a systematic method to estimate the GWP solely from molecular structure for refrigerants. The feasibility to extend these methods to siloxanes and other working fluids must be investigated in detail.

6. *Toxicity* should be as low as possible and can be calculated by using group contribution methods that were developed based on the acute toxicity of chemical substances [13].

7. *Lower Flammability Limit* at the turbine inlet temperature and pressure must be as high as possible to prevent the ignition of the working fluid. Kazakov et. al. [51] have developed a method to estimate this limit based on the enthalpy of formation for refrigerants. The application of this technique to working fluids such as siloxane must be investigated and is out of the scope of this work.

8. *Maximum Operating Pressure* should be generally moderate in order to save the costs of using expensive equipment.

9. *Minimum Condensing Pressure* should be high enough to design a finite sized condenser.

10. *Maximum Flow-rate* should be low to reduce operating costs

11. *Thermal Stability* of the fluid should generally be high.

Table 3-6 summarizes the above points which can be considered as performance measures. The optimization problem is oriented to the design the system, and it is focused on the

Table 3-6: Fluid and system performance measures (adapted from Papadopoulos et. al. [13])

Thermodynamic	**Environmental**	**Safety**	**System-related**
Density	Ozone Depletion Potential (ODP)	Toxicity	Net Power Output
Specific Heat Capacity	Global Warming Potential	Flammability	Maximum operating pressure
Viscosity			Mass flow-rate
Thermal Conductivity			Minimum Condensing Pressure
Thermal Stability			

maximization of the output power. The working fluids are limited to the family of siloxanes which have high thermal stability, high density, suitable critical point for high-temperature

ORC applications, availability, and moderate cost. They are also considered as non-ozone-depleting in the stratosphere, and have negligible global warming potential due to their short atmospheric lifetimes thus complying to the environmental performance limits [52, 53]. In addition, they have good lubricating properties; thus allowing for lubrication of the turbine shaft by means of the working fluid itself, greatly simplifying the overall system [21]. Thus by limiting to the class of siloxanes, most of the fluid performance measures have been accounted for and hence can be excluded from the objective function. This allows the net output power to be defined as the single objective function within the scope of this work.

3-6 Design of Experiments

Design of Experiments is a general term to denote any method available for setting parameter values in a certain domain of interest forming a set of experiments or sample points [54]. The primary goal of such an exercise is to extract the maximum amount of unbiased information about the objective function from as few observations as possible [55]. There are several methods to generate a set of sample points such as Random Allocation, Optimal Latin Hypercube design, Optimal Latin Square design, Cubic Face Centered design, Box-Behnken, etc. In this work, the Optimal Latin Hypercube design procedure has been chosen to generate inputs for the optimization algorithm. The sample points are created using a two level pseudo random

Table 3-7: Parameters for the Optimal Latin Hypercube allocation

Tuning Parameter	Value
Number of Points	200
Seed	1000
Base Generator	Centered Point
Distribution	Uniform
Point Combiner	Entropy
Maximum Iterations	100
Maximum No Improvement Iterations	15
Optimization Algorithm	Iterated Local Search

process wherein each dimension is randomly sampled according to a predefined distribution in the first level and then recombined to form the final design in the second level. The recombination of points in the second pseudo level undergoes an optimization process in order to spread the points as evenly as possible within the design space based on the entropy criteria. A centered point generator with a uniform distribution is used to generate the first pseudo level of points. An entropy point combiner is used to recombine the points with an objective to minimize the entropy of system [54]. The entropy of the system is computed as:

$$S = -ln\left(det\left(C\right)\right) \tag{3-14}$$

where C is the correlation matrix of the N sample points defined as:

$$c_{ij} = exp\left\{-2\left(x_i - x_j\right)\right\} \tag{3-15}$$

The entropy point combiner operates on all the points of the system at the same time and tries to minimize the correlation matrix using an optimization algorithm called the Iterated Local Search [54]. Figure 3-14 presents a pictorial representation of the iterated local search algorithm.

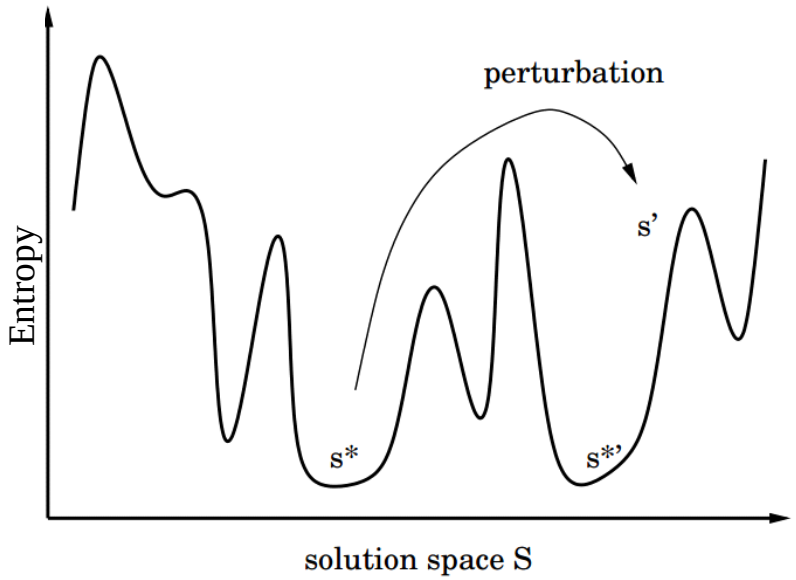

Figure 3-14: Pictorial representation of iterated local search (adapted from Kochenberger et. al. [56])

Starting with a local minimum entropy s^*, a perturbation is applied leading to an entropy $s^{'}$. A local search is then applied to find the local minimum which is represented by $s^{*'}$. The values of s^* and $s^{*'}$ are then compared to find the new minimum value of entropy. This procedure is carried out iteratively to minimize the entropy of the system and generate the required sample points which are then used as inputs to the optimization algorithm described in the following section.

3-7 Optimization Algorithm

Table 3-8: Control parameters for the SOGA

Tuning Parameter	Value
Iterations	250
Population Size	20
Crossover probability	0.5
Crossover kind	Full weight
Mutation probability	0.1
Mutation kind	Uniform
Seed	1000

An evolutionary algorithm, called Genetic Algorithm (GA), has been used which is effective regardless of the shape of the objective function and the constraints. The algorithm combines the use of random numbers and information from previous iterations to evaluate and improve a population of points (a group of potential solutions) rather than a single point at a time. Based on the theory of the natural selection in the biological genetic progress which was developed by Charles Darwin, the GA features a fast sorting procedure and an elitism preservation mechanism which preserves the most optimum fitness during each iteration [57].

The design variables are evaporator pressure, condenser pressure and the segment number. These variables are encoded onto a chromosome (design vector) and an initial population of designs is randomly generated. The population generated serves as an input to the GA where three basic operations are applied: selection, crossover and mutation [57].

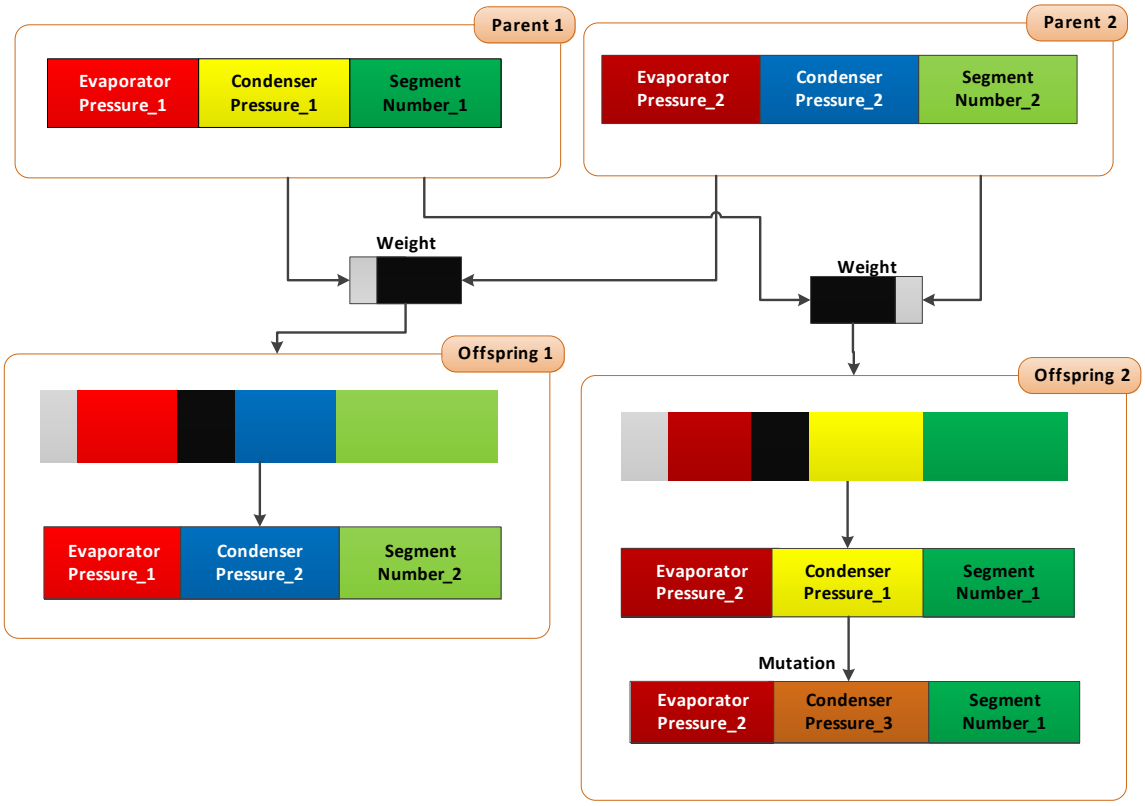

Figure 3-15: An illustration of crossover and mutation operations for the GA

Selection involves selecting chromosomes from the current population which will be used in the generation of the next population based on its fitness value. This value is determined by a function and is an indication of how desirable the chromosome is in terms of surviving into the next generation. The design of experiments described previously is used to generate the initial population of chromosomes. Once a chromosome is selected, crossover operation is performed in which two designs from the previous population (parents) are combined to design new offspring. A full-weight crossover setting is used with a probability of 0.5. The offspring chromosome is altered randomly in the operation called mutation which intends to introduce variations into the population. A uniform mutation with probability of 0.1 is used in this work. Figure 3-15 provides an illustration of the crossover and mutation operations which occurs in the GA.

The procedure is repeated until the objective function is maximized. Figure 3-16 illustrates the flowchart of the GA.

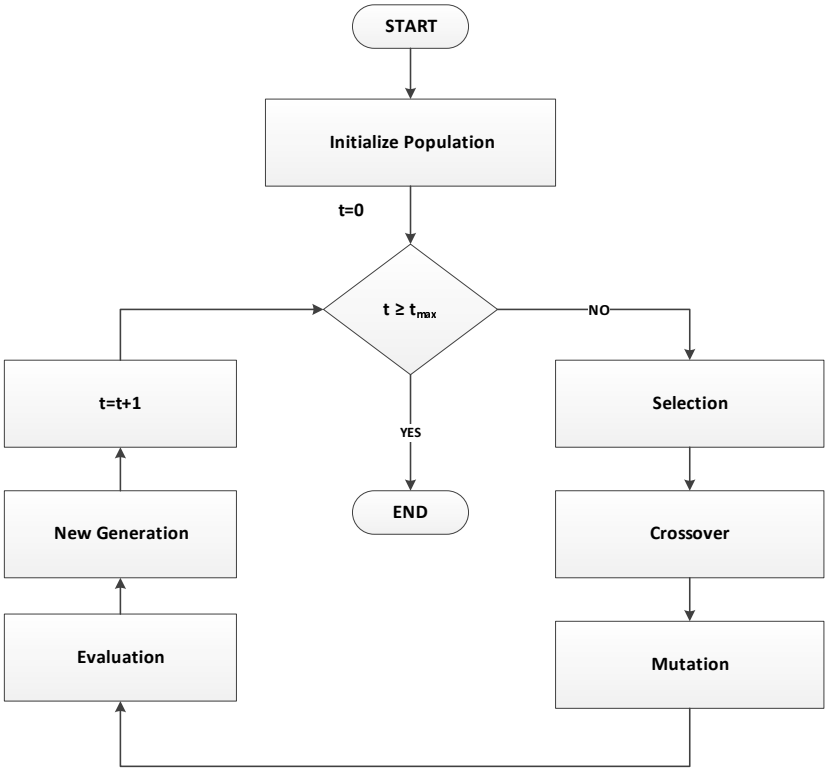

Figure 3-16: A flowchart illustrating the genetic algorithm (adapted from van den Braembussche [58])

Table 3-9: Constraints implemented for the GA

Parameter	Target Value
Segment Number (m) $[-]$	$4 \leq m \leq 8$
Evaporator Pressure (P_E) $[bar]$	$1 \leq P_E \leq 40$
Evaporator Temperature (T_E) $[^oC]$	$T_E > 0$
Condenser Pressure (P_C) $[bar]$	$0.05 \leq P_C \leq 1$
Condenser Temperature (T_C) $[^oC]$	$T_C > 85$
Pinch Point Temperature Difference in Evaporator ΔT_p $[K]$	$\Delta T_p > 5$
Cooling water flow rate (Vcw) $[l/s]$	$0 \leq Vcw \leq 1$

3-8 Constraints

The optimization variables viz. segment number, evaporator pressure and condenser pressure have been constrained. The segment number has been restricted to limit the scope of the fluid search to siloxanes. From Table 3-1, it is clear that the segment number for such fluids should be constrained between 4 and 8. The evaporator pressure is bound to be lower than 40 bar which is the technological limit for small plate heat exchangers suitable for such applications [21]. The lowest possible pressure in the condenser is considered to be 0.05 bar in order to provide the necessary sealing to prevent the atmospheric air to enter the system [21]. A minimum pinch point temperature difference between hot and cold fluid is set to 5 K to ensure compact evaporator heat exchangers. The condenser temperature is limited to

be above 85^oC as the cooling water enters the condenser at a temperature of 80^oC. The cooling water flow rate in the truck's cooling system has been limited to a maximum of $1l/s$. Table 3-9 summarizes the above discussion.

3-9 Structure Mapping

The segment number has been considered as the only optimization variable from the fluid component parameters of the PCP-SAFT model. Hence a simple selection based on the distance between the hypothetical and real segment numbers has been done. The design of the CoMT-CAMD approach described above has been implemented in the form of a software tool. The following section presents the architecture for the same.

3-10 Implementation into a software tool

The ORC system described earlier has been modeled in Cycle-Tempo [8]. The process parameters are written on a series of input files called INFILE1, INFILE2, INFILE3 and the outputs from the system simulation are written onto a series of output files called OUTFIL1, OUTFIL2, OUTFIL3 and OUTFIL4. Cycle-Tempo allows the user to specify the working fluid and the thermodynamic model. The hypothetical fluid parameters are written onto a text file identified by *.saf* extension. This fluid is then used as a working fluid in the ORC system. Cycle-Tempo calls FluidProp [37] when the system simulation is carried out.

The radial turbine model described in the previous section has been implemented into the calculation core of Cycle-Tempo. The GA has been implemented into a state of the art optimization suite called Nexus (version 2.1) [20]. The system optimization variables viz. evaporator and condenser pressures are defined as continuous variables in Nexus and written onto the INFILE1 of Cycle-Tempo.

The segment number being the fluid optimization variable, is used to calculate the other parameters of the PCP-SAFT model based on the expression defined earlier. These parameters are then written onto the fluid file through Nexus. The objective function i.e. net power output is read from the OUTFIL4 along with other cycle parameters. The tool interacts with MATLAB [59] in which the functions to calculate the evaporator pressure and the pinch point temperature difference have been implemented. Figure 3-17 illustrates the entire programming framework and the relations between Cycle-Tempo, FluidProp, MATLAB and Nexus.

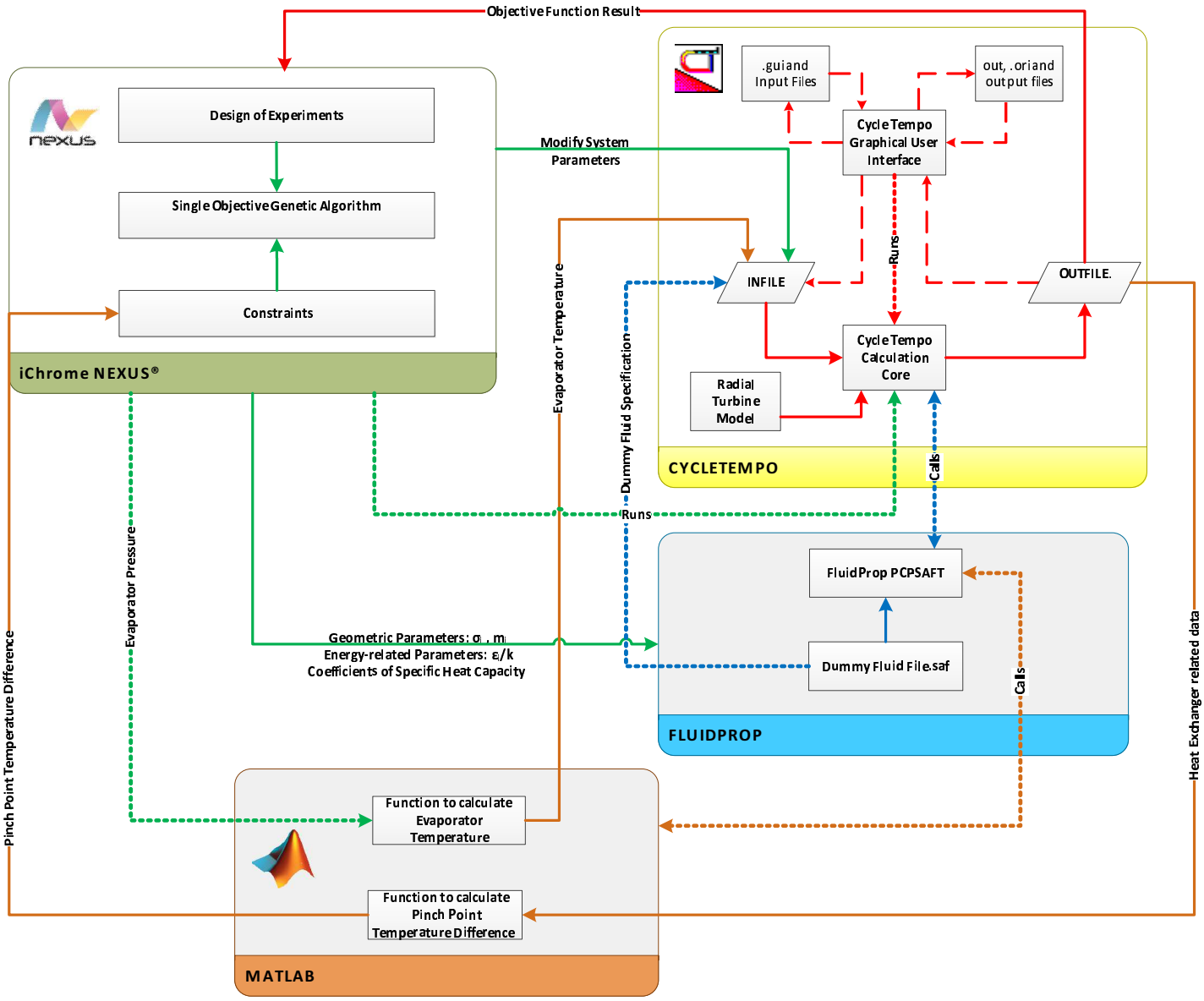

Figure 3-17: An illustration representing the architecture of the tool

Chapter 4

Results and Discussion

The following chapter presents the results and discussion of the optimization problem defined in Chapter 3. The validation of the ORC turbogenerator model and the thermodynamic model have been presented followed by results of the optimization and the turbine models. The influence of the turbine model on the optimization problem has also been discussed.

4-1 System model validation

The ORC turbogenerator model has been developed in Cycle-Tempo which is based on the work of Lang et. al. [21] with the input parameters as mentioned in the previous chapter. The simulated results of this model from Cycle-Tempo has been validated against the same paper. Table 4-1 presents a comparison of these results. The mass flow rate and the net

Table 4-1: Comparison of the system model with reference model

	This Work	**Lang et. al. [21]**
Segment Number [-]	5.7535	5.7535
Evaporator Pressure [bar]	3.920	3.920
Condenser Pressure [bar]	0.087	0.087
Condenser Temperature [^oC]	100.27	100
Turbine Inlet Temperature [^oC]	242.5	242.5
Total Mass Flow rate [kg/s]	0.246	0.266
Turbine Efficiency [%]	81.05	78
Thermal Power-Exhaust evaporator [kW]	25.32	27.4
Thermal Power-EGR evaporator [kW]	31.45	34.2
Net Output Power [kW]	9.32	9.6
Net Efficiency [%]	16.42	15.6

power output in this work are lower than the reference work. It is also worth noting that a lower net thermal power is transferred in the model developed in this work. One of the reasons for the difference in the net thermal power transferred can be related to the flue gas composition chosen for this model. The flue gas is assumed to have a composition based on a diesel engine used in the work of Bombarda et al. [38] while Lang et al. have determined the

composition from engine performance maps [21]. Another reason for this difference could be due to the fact that the paper does not consider the pressure drops in the heat exchanging equipments. The turbine model implemented influences the mass flow rate of the working fluid which in turn affects the net power output of the ORC system. The net efficiency is, however, higher because the input power to the system is lower (57 kW_{th}) than the work of Lang et al. (62 kW_{th}) in addition to a higher turbine efficiency. The system model developed here is then optimized along with the fluid parameters. However, before proceeding onto the optimization results, it is essential to validate the thermodynamic model implemented. The following section presents this comparison.

4-2 Validation of Thermodynamic model

The fluid parameters of the PCP-SAFT EOS have been derived by fitting them to the segment number as described in Chapter 3. A model to calculate the ideal gas heat capacity coefficients has also been proposed. It is important validate the model before proceeding onto the optimization problem. The PCP-SAFT model in FluidProp [37] is chosen as the reference against which this work has been validated. Table 4-2 presents a comparison of the simulated fluid parameters with those from FluidProp.

Table 4-2: Comparison of the simulated fluid parameters

	MDM (This Work)	MDM (FluidProp [37])
Segment number [-]	5.15037	5.15037
Molecular Mass[kg/kmol]	246.343	236.53
Segment diameter [Å]	4.1038	4.16893
Segment energy parameter ϵ/k [K]	211.915	213.3824
A [J/molK]	69.4034	-6.16409
10^3 B [J/molK^2]	991.4745	1184.23
10^6 C [J/molK^3]	-556.495	-679.873
10^9 D [J/molK^4]	93.6186	145.228

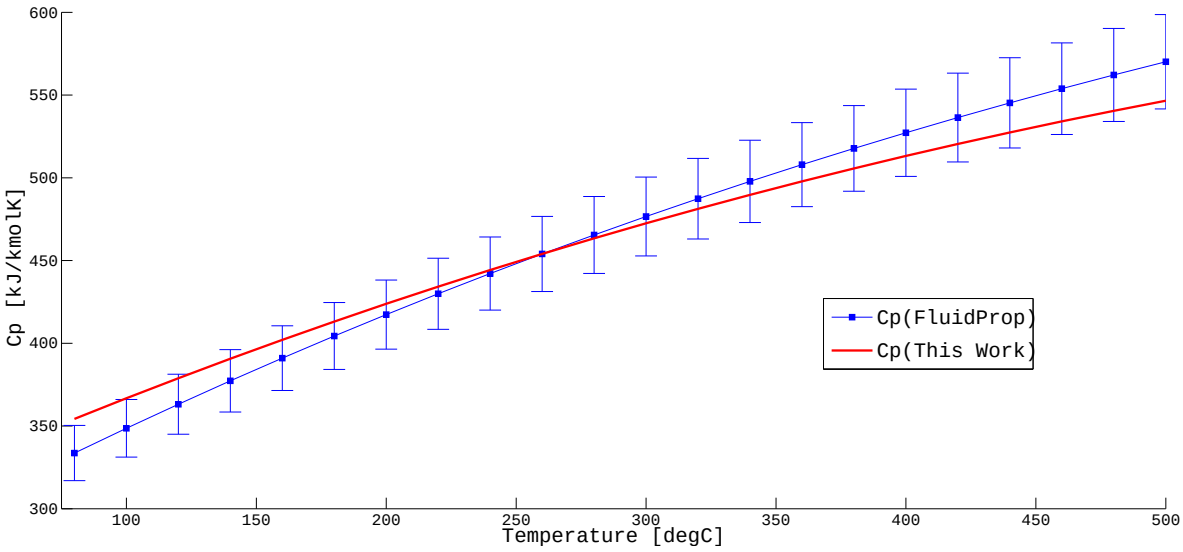

Figure 4-1: Comparison of the specific heat capacities for relevant temperature range for MDM

The relative error between the pure component parameters of this work and FluidProp is less than 4% which is reasonable. The coefficients of ideal gas heat capacity differ in their magnitude but the overall heat capacity calculated from both the coefficients show a variation of only 1-5% for the given temperature range. Figure 4-1 illustrates the comparison of the specific heat capacity at constant pressure from this work and FluidProp for MDM. This variation in the specific heat capacity is acceptable as the values of siloxanes available in literature have an uncertainty of about 5% [60]. The difference in the specific heat is reflected onto the output power which has a relative error of around 3% when compared to the power output obtained using the default fluid MDM available in FluidProp. Based on the system and the thermodynamic model, the results of the optimization was obtained which has been presented in the following section.

4-3 Analysis of the simulated optimized ORC Turbogenerator

A design of experiments procedure was implemented in order to generate the required input population for the genetic algorithm. The following section analyses the results of this procedure.

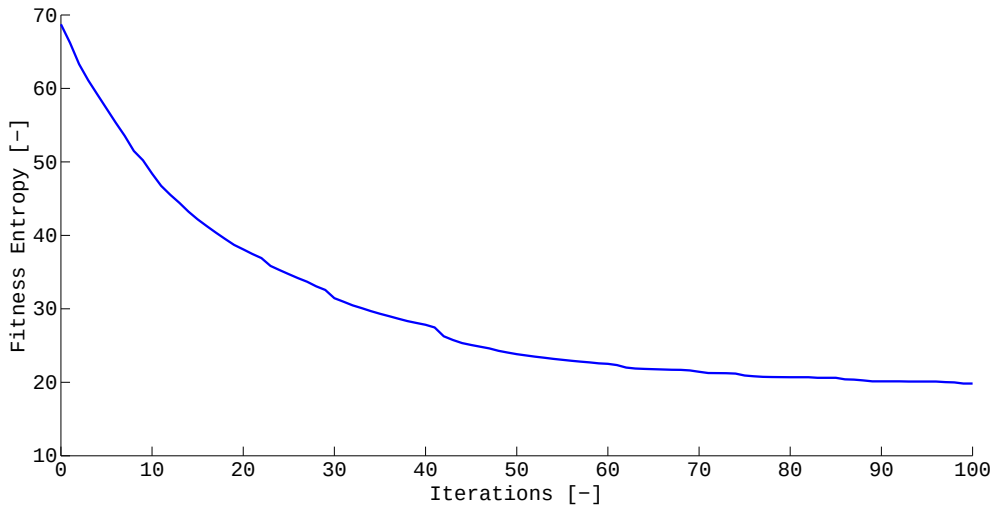

Figure 4-2: Fitness entropy during each iteration in Latin Hypercube Sampling

4-3-1 Analysis of design of experiments

The Optimal Latin Hypercube Sampling procedure, described in the previous chapter, generates a set of initial sample points based on the entropy criteria. Figure 4-2 illustrates the minimization of this entropy over 100 iterations. The sample points are then generated such that the fitness entropy of the set of optimization variables is equal to the minimum entropy after 100 iterations. Figure 4-3 illustrates the result of this sampling procedure. From the figure, it is seen that the value of the optimization variables are spread over the whole domain

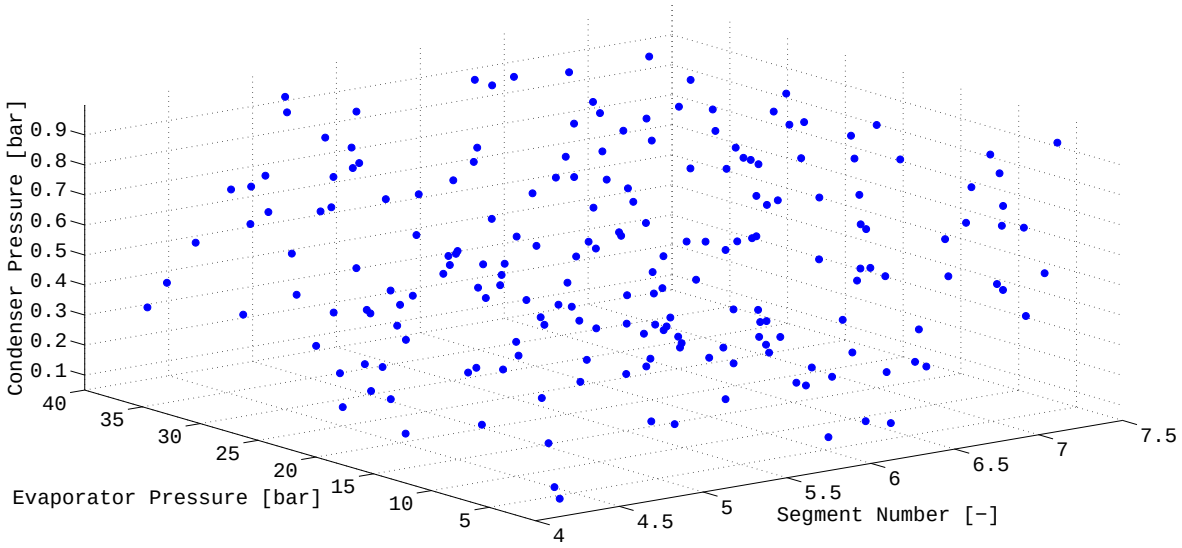

Figure 4-3: Latin Hypercube Sampling result

and hence, the probability of missing out on the optimum set of input values reduces. Based on these initial points, the optimization is run and the following section presents these results.

4-3-2 Optimization Results

The CoMT-CAMD, as described earlier, has two steps. Thus the optimization procedure can be visualized as a two step problem. In the first step, the optimization of the process and fluid parameters leads to a hypothetical working fluid with segment number of 4.62 with a net output power of 10.09 kW. Figure 4-4 illustrates the value of the best objective function during each iteration.

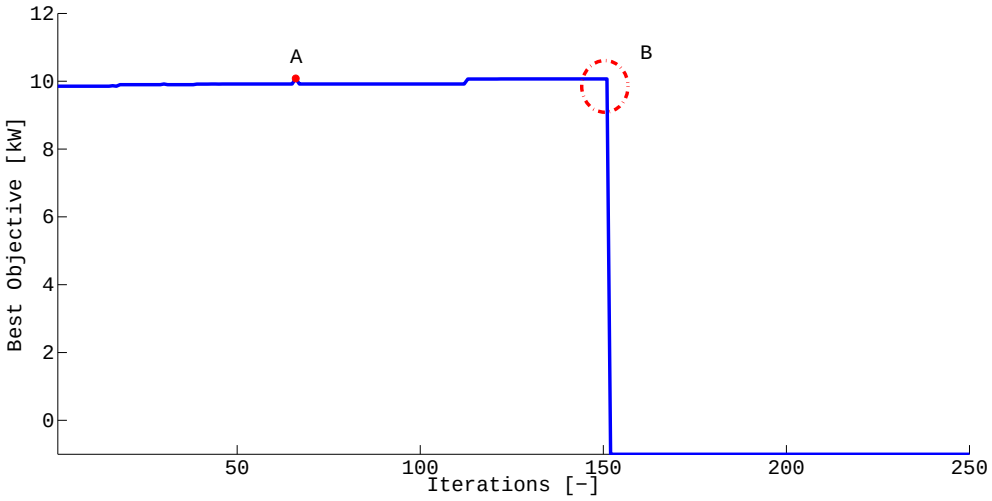

Figure 4-4: Best objective function during each iteration

The best objective is achieved after 66 iterations which is represented by point A in the figure. The point B in the figure is interesting because after 150 iterations, the tool is unable to calculate the net output power. This limitation is mainly because of the limit on the number of fluids allowed in FluidProp database. FluidProp uses a fluid table to read the corresponding fluid files. This fluid table can only contain 1000 lines, implying 1000 fluids. Since the tool generates a unique hypothetical fluid file for each chromosome of the optimization variables, the number of hypothetical fluids exceeds the limit after 150 iterations. However, since the best objective is found to be well before point B, it is safe to claim that the optimum value of fluid and process parameters are achieved. Figure 4-5 illustrates a step-wise variation of the maximum net output power with respect to the number of iterations.

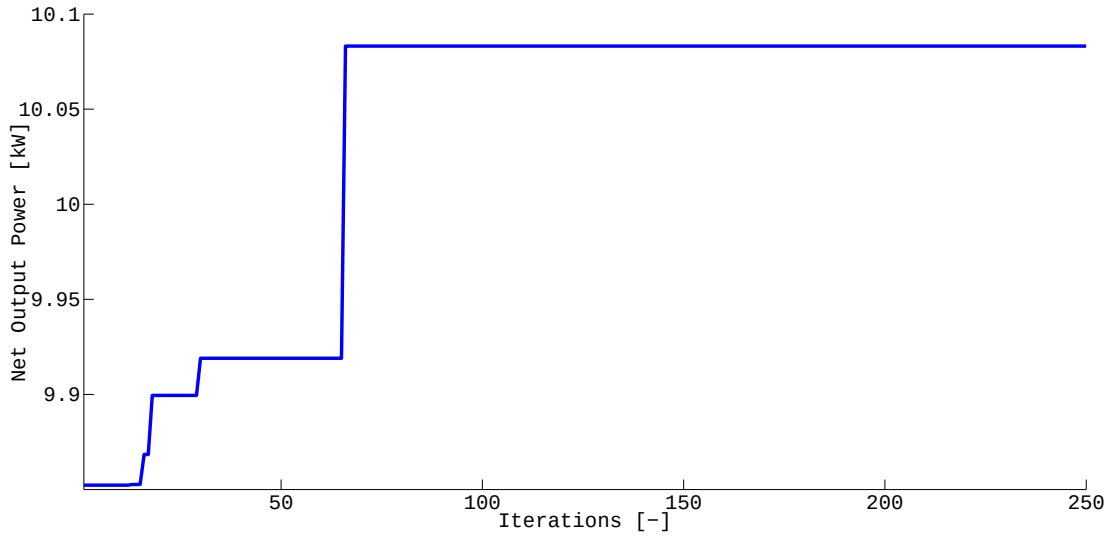

Figure 4-5: Variation of the output power with number of iterations

Thus the resulting optimum fluid is hypothetical and hence has to be mapped onto a real fluid based which is the second step of the CoMT-CAMD method outlined previously in Chapter 3. From Table 3-1, it is clear that the closest real fluids from the siloxane family are MM and MDM. The second step of the optimization process is thus to optimize the process again while keeping the fluid fixed to MM or MDM. The optimization process was run for both the fluids. The optimum ORC system running on MM has a maximum net output power of 10.20 kW which is high when compared to the system running on MDM which has a net output power of 9.77 kW and also higher than the optimum hypothetical fluid. The power output in case of MM is higher than the optimum hypothetical fluid because of a higher turbine inlet temperature. The preliminary turbine design for MM resulted in a turbine with a rotor diameter of about 37 mm and speed of revolution of about 133,858 rpm. Imoberdorf et. al. [61] present the application areas and limits of speed of revolution with respect to the output power illustrated in Figure 4-6.

From the figure, it can be inferred that the speed of revolution, in case of MM, is very close to the technological limit of magnetic bearings for the range of output power obtained in this system. Furthermore, the optimum system with MM has a maximum cycle pressure of 20.78 bar. In case of MDM, the maximum speed of revolution from the preliminary turbine design is around 66780 rpm with a rotor diameter of 68 mm which is further away from

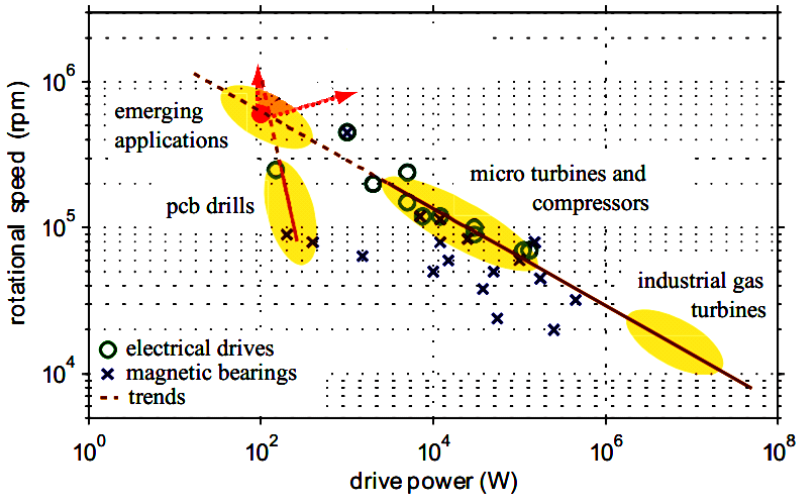

Figure 4-6: Application areas for ultra-high-speed drives and magnetic bearing (from Imoberdorf et. al. [61])

the technological limit when compared to MM. Also, the optimum MDM cycle operates at a significantly lower maximum pressure of 8.5 bar. Although the ORC system with MM as a working fluid results in a higher output power in the ORC system than MDM but the magnitude of gain (0.43 kW) is considerably less if the cost of the system with such high pressures and high speed turbine are taken into consideration.

Although the optimum working fluid for this system based on the tool is MM, MDM is chosen as the real optimum fluid based on the above arguments. Table 4-3 shows a comparative analysis of the optimized ORC turbogenerator, with hypothetical and real optimum fluids, with the system running on D4 based on Lang et al.[21]. The T-s diagrams comparing the three fluids has been illustrated in Figure 4-7

Table 4-3: Comparative analysis of the simulated optimized ORC turbogenerator

	Hypothetical Optimum Fluid	**Real Optimum Fluid (MDM)**	**D4**
Segment Number [-]	4.62	5.15037	5.7535
Evaporator Pressure [bar]	15.62	8.45	3.920
Condenser Pressure [bar]	0.483	0.200	0.087
Condenser Temperature [^oC]	97	96.54	100.27
Turbine Inlet Temperature [^oC]	260.82	255.2	242.5
Total Mass Flowrate [kg/s]	0.213	0.225	0.247
Thermal Power-Exhaust evaporator [kW]	26.31	24.64	25.32
Thermal Power-EGR evaporator [kW]	32.01	31.07	31.45
Net Power [kW]	10.09	9.77	9.32
Net Efficiency [%]	17.30	17.54	16.42

From the table it is clear that the net output power for MDM is more than D4. This is because of the higher turbine inlet temperature caused by a higher evaporator pressure and a lower condenser temperature. The net efficiency is also higher for MDM as the power produced is higher even when as the net thermal power to the system is lower. A higher condensing temperature might have been selected in the work of Lang et al. [21] as condensing pressures lower than the technological limit are obtained for lower temperatures [28]. In case

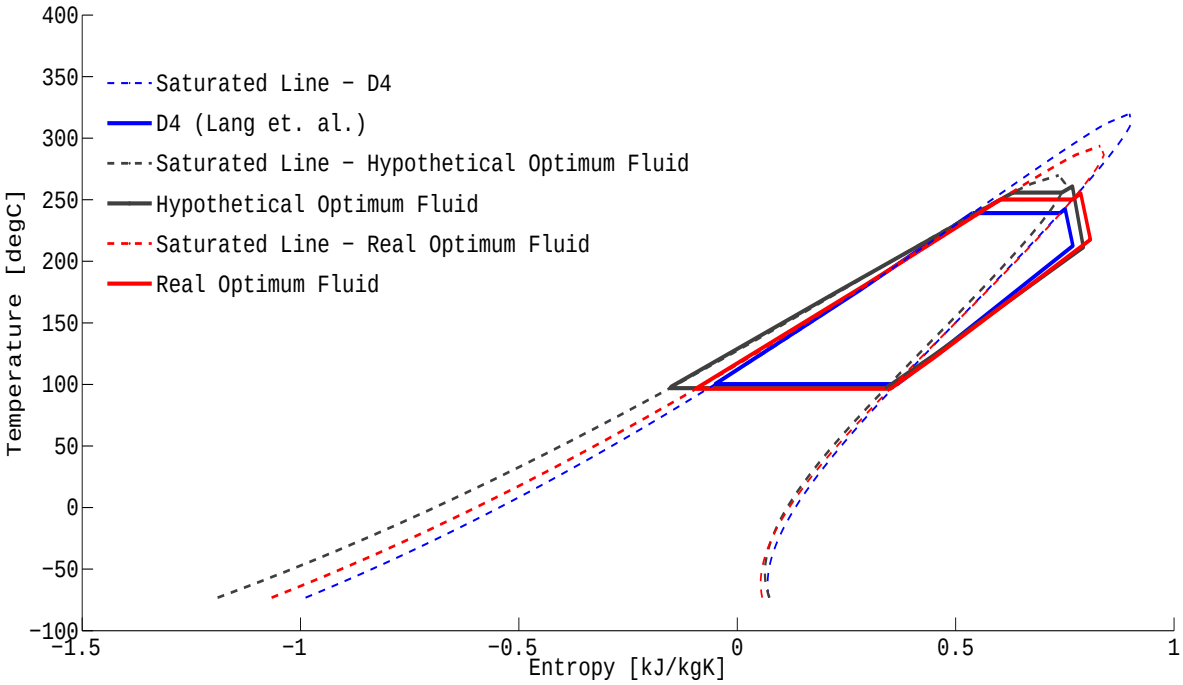

Figure 4-7: Comparison of T-s Diagrams for the optimized fluids and D4

of MDM, the condenser pressure is higher when compared to D4 because of its higher critical pressure. The cooling water enters the condenser at 80^oC. The constraint on the volumetric flow rate of this cooling water as mentioned, in the previous chapter, leads to such higher condensing temperatures. The evaporator pressure in case of MDM is higher than D4. The higher evaporator pressure leads to a higher cycle efficiency which also leads to a higher turbine outlet temperature. Thus the amount of regeneration increases leading to higher temperatures at the evaporator inlet. This limits the exhaust temperature of the flue gases to increasingly higher values and does not improve the amount of heat recovered from the exhaust. Thus there should be a trade-off between the evaporator pressure and the net output power as the gain in output power in case of MDM is only 0.4 kW while the net thermal power recovered decreases for MDM by around 1 kW_{th} with a change in evaporator pressure of around 4.5 bar which may affect the cost of the heat exchangers. Depending on further system design, the electrical power can be used by other on-board systems, or stored in batteries. Alternatively the turbine shaft can be connected to the engine crankshaft using a gearbox [21].

4-4 Turbine Results

The following section presents the results of the radial turbine model described earlier in Chapter 3. Table 4-4 shows a comparison of the performance of the radial turbine with the hypothetical and optimum fluids against the work of Lang et al.[21]. The model implemented in this work is based on non-dimensional parameters while Lang et. al. uses the turbine model based on the design methodology outlined by Whitfield and Baines [1]. The paper uses an impulse type radial turbine which imposes a zero degree of reaction on the turbine

Table 4-4: Comparative analysis of the turbine results

	Hypothetical Optimum Fluid	Real Optimum Fluid	D4[21]
Speed [rpm]	103129	66880	25990
Specific Volume Ratio [-]	54.62	57.69	53
Specific Pressure Ratio [-]	32.03	41.16	45.06
Blade height at nozzle outlet [mm]	1.25	1.69	2.8
Rotor inlet diameter [mm]	47	68	160
Rotor out rms diameter [mm]	25	37	90
Isentropic Efficiency [%]	81.22	81.13	78
Mach number at rotor inlet M_{w2} [-]	1.59	1.67	1.66*
Mach number at rotor outlet M_{w3} [-]	0.75	0.79	0.92

* Quoted as M_{abs2} in [21]

while a low degree of reaction has been considered for reasons stated in the previous chapter. The speed of revolution of the turbine for the optimum fluid is considerably higher than the reference work. One of the reasons for this could be the molecular weight which is lower in case of MDM than D4. The total mass flow decreases by around 9% in case of MDM . Thus in order to achieve volumetric flow rates of the same order, the turbine with MDM as working fluid has to rotate at a much higher rpm than D4. The resulting turbine has a significantly smaller rotor diameter thus making the system compact and feasible to be implemented on board a truck. The specific speed is best regarded as a shape parameter that for any given value there is an optimum rotor form [1]. The specific speed of the turbine in case of MDM is 0.8. Rohlik [45] predicted a distribution of losses along the curve of maximum total to static efficiency of the turbine with respect to the specific speed which is shown in Figure 4-8.

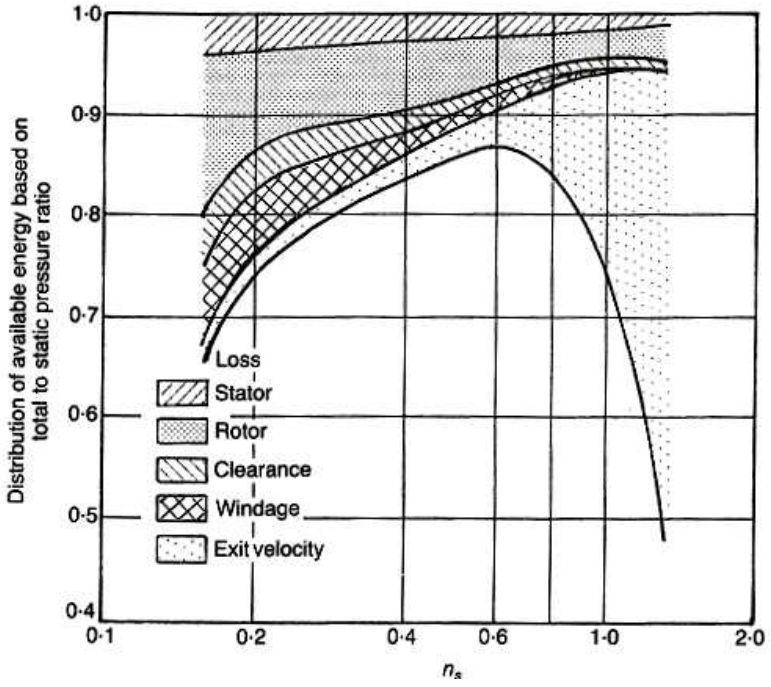

Figure 4-8: Predicted distribution of losses along the curve of maximum total to static efficiency [45]

The majority of the losses that are present at a specific speed of 0.8 is due to the exit

velocity. This also confirms the fact that an efficient diffuser was not designed and hence its beneficial effects were ignored in this work.

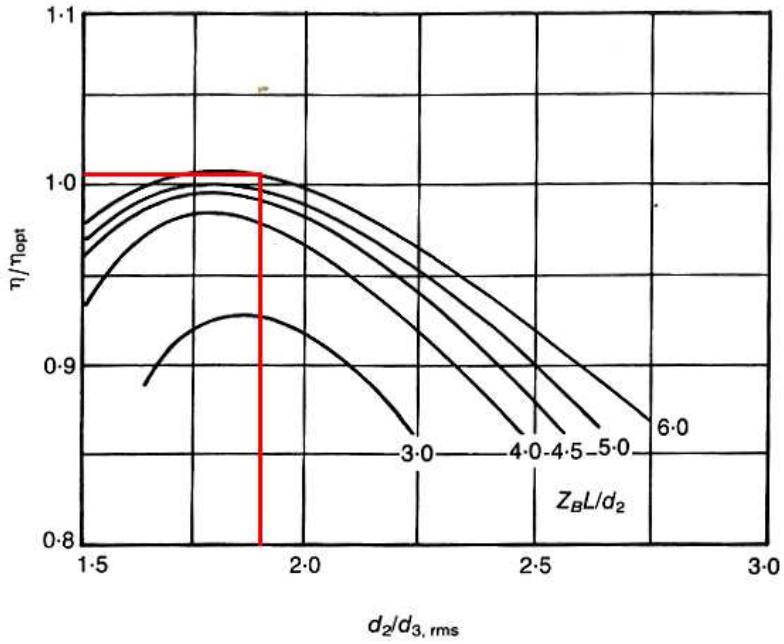

Figure 4-9: The effect of rotor diameter ratio and blade solidity on radial turbine efficiency(from Rodgers and Geiser [42])

Another important factor which determines the design of the rotor is the blade solidity which is the measure of the strength of the blade given by the equation:

$$Solidity = \frac{Z_B L}{D_2} \tag{4-1}$$

where Z_B is the number of vanes, L is the rotor axial length and D_2 is the rotor diameter at the inlet. The solidity of the blade has a significant effect on the isentropic efficiency of the turbine. A low solidity would mean that the deviation of the efficiency from the optimum would be about 8%. In this work, the turbine has a solidity of 6 with a diameter ratio of 1.85. Thus from Figure 4-9, it is seen that the efficiency is slightly over estimated with respect to the optimum. The number of vanes, Z_B, can be evaluated based on Glassman's equation [62] which is an empirical relation between the number of vanes and the nozzle outlet angle, α_2 and is expressed as:

$$Z_B = \frac{\pi}{30}(110 - \alpha_2)\ tan\alpha_2 \tag{4-2}$$

Using equations (4-1) and (4-2), the axial length of the rotor can be evaluated. The value of this axial length was found to be around 60 mm. The relative Mach number at the nozzle outlet is 1.59 which is greater than 1 and hence there is possibility that the uncertainty due to the supersonic flow at the rotor inflow would result in a lower efficiency, due to shock waves impinging on the rotor blades [63], though a more refined aerodynamic design might lead to shockless turbine operation in design conditions. Other factors that might influence the turbine fluid dynamic performance are the effects of tip clearance and windage losses [21] which are out of the scope of this work.

Uusitalo et. al. [28] state that the selection of the working fluids should be based on the optimization of the overall conversion performance, rather than solely on the optimization of the turbine efficiency. Thus in order to investigate the influence of the turbine model on the optimization process, the tool is run with a constant efficiency turbine. The following section presents the influence of the turbine model.

4-4-1 Influence of the turbine model

The optimization of the process and fluid was carried out for a turbine with a constant efficiency of 78%. Table 4-5 presents a comparison of the two cases.

Table 4-5: Influence of turbine model on the optimization

	Radial Turbine Model	Constant Efficiency Turbine
Segment Number [-]	4.621	4.618
Evaporator Pressure [bar]	15.62	16.69
Condenser Pressure [bar]	0.483	0.486
Condenser Temperature [^oC]	97.00	97.02
Turbine Inlet Temperature [^oC]	260.82	264.87
Total Mass Flowrate [kg/s]	0.213	0.211
Thermal Power-Exhaust evaporator [kW]	26.31	25.68
Thermal Power-EGR evaporator [kW]	32.01	31.65
Net Power [kW]	10.09	9.67
Net Efficiency [%]	17.30	16.87

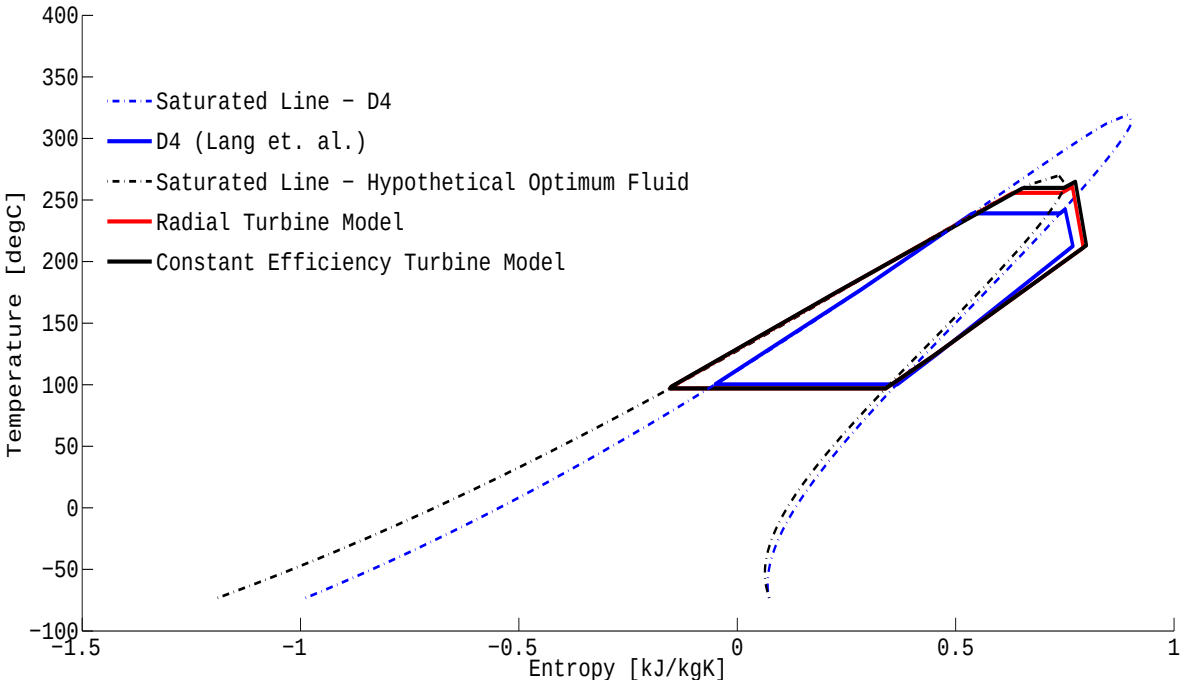

Figure 4-10: T-s diagram for optimal fluids with different turbine models and D4

Figure 4-10 illustrates the T-s diagrams for optimal fluids with different turbine models and has been compared to D4. From the figure and Table 4-5, it is seen that in the scope of the present work, the turbine model does not influence the selection of the optimum hypothetical

fluid and the process parameters. The only significant difference is the slightly lower power output and net efficiency. The final selection of the working fluid should be based on the optimization of the overall conversion performance, rather than solely on the optimization of the turbine efficiency. However, it should be noted that lower turbine efficiencies increases the load on the condenser [28]. The incorporation of a preliminary design model gives an idea of the dimensions of the turbine and governs the optimization and hence is recommended.

4-5 Heat Exchanger results

Table 4-6: Comparative analysis of the heat exchanging equipment results

	Hypothetical Optimum Fluid	Real Optimum Fluid	D4
Exhaust gas evaporator			
Heat Transmitted [kJ/s]	26.31	24.64	25.32
High terminal temperature difference[^oC]	46.18	51.80	64.5
Low terminal temperature difference [^oC]	25	25	25
Pinch point temperature difference [^oC]	21.75	16.83	25
UA [W/K]	0.762	0.669	0.608
EGR evaporator			
Heat Transmitted [kJ/s]	32.01	31.07	31.45
High terminal temperature difference[^oC]	168.18	173.80	186.50
Low terminal temperature difference [^oC]	25	25	25
Pinch point temperature difference [^oC]	25	25	25
UA [W/K]	0.426	0.405	0.391
Condenser			
Heat Transmitted [kJ/s]	47.89	45.61	47.15
High terminal temperature difference[^oC]	5	5	5
Low terminal temperature difference [^oC]	17.00	16.54	20.27
Pinch point temperature difference [^oC]	5.00	5.00	5
UA [W/K]	4.88	4.73	4.32
Regenerator			
Heat Transmitted [kJ/s]	32.33	35.50	33.88
High terminal temperature difference[^oC]	37.87	37.21	35.42
Low terminal temperature difference [^oC]	25	25	25
Pinch point temperature difference [^oC]	25	25	25
UA [W/K]	1.043	1.156	1.133

Table 4-6 presents a comparison of the heat exchanging equipments for each fluid. As discussed earlier, the higher evaporator temperatures in the optimal fluids reduces the amount of heat that can be extracted from the flue gas. Hence the heat transmitted is lower in case of the optimal fluids when compared to D4. Also, the condenser has the highest UA value among all the heat exchangers which implies a larger area is required. This is mainly because of the high volumetric flow due to relatively lower density from the turbine outlet which has to be cooled.

Figure 4-11 illustrates a comparison of the Q-T diagrams for the evaporators with respect to the work of Lang et. al. [21] who provide only one diagram for the evaporator and hence it is assumed to be the exhaust gas evaporator. The pinch point temperature difference is lower in this work for the exhaust gas evaporator illustrated in Figure 4-11(a) when compared to the work of Lang in Figure 4-11(c). The exhaust gas heat exchanger has a lower exergy loss than the evaporator designed in the paper. The exergy loss is considerably higher in the EGR evaporator as both the evaporators are assumed to have the same pressure and outlet temperature. This loss can be reduced by varying the pressure and temperature in the EGR evaporator but it can lead to issues in control of the system.

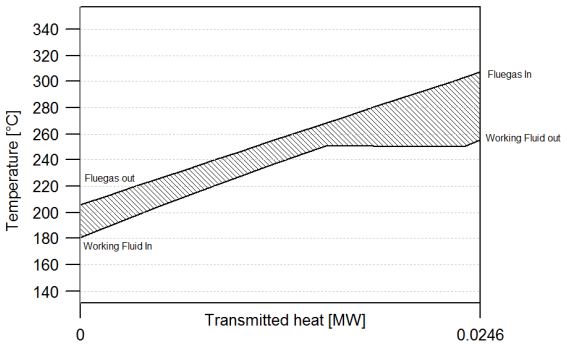

(a) Exhaust gas Evaporator (This Work)

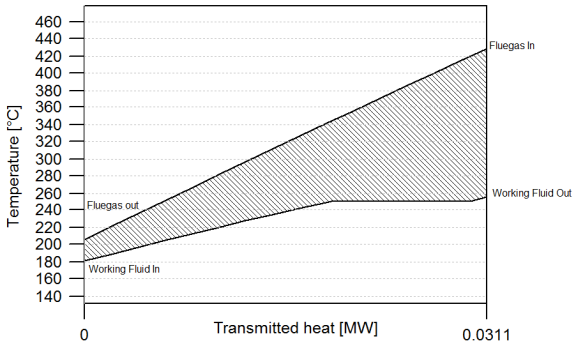

(b) EGR Evaporator (This Work)

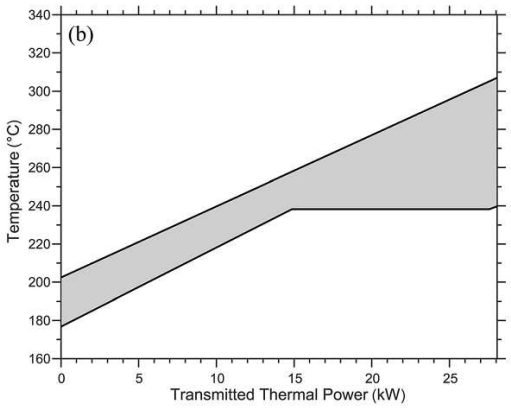

(c) Evaporator (Lang et. al. [21])

Figure 4-11: Comparison of Q-T diagrams for evaporators

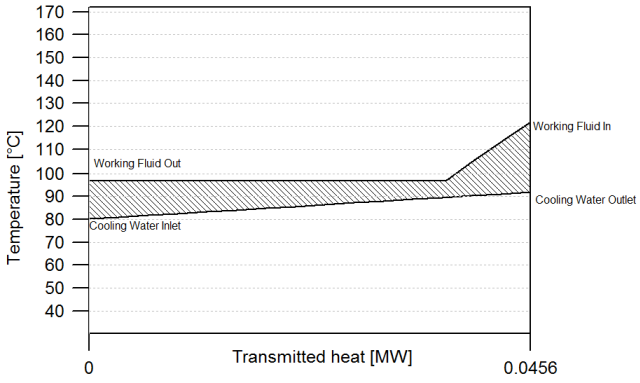

(a) Condenser (This Work)

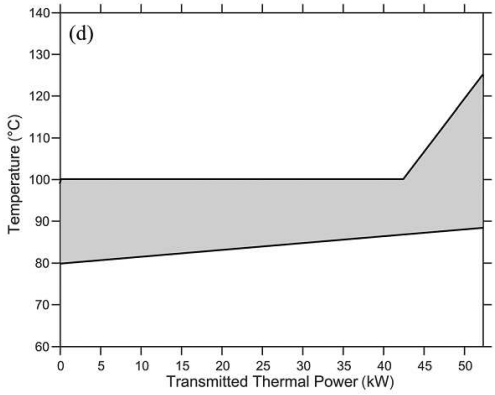

(b) Condenser (Lang et. al. [21])

Figure 4-12: Comparison of Q-T diagrams for condensers

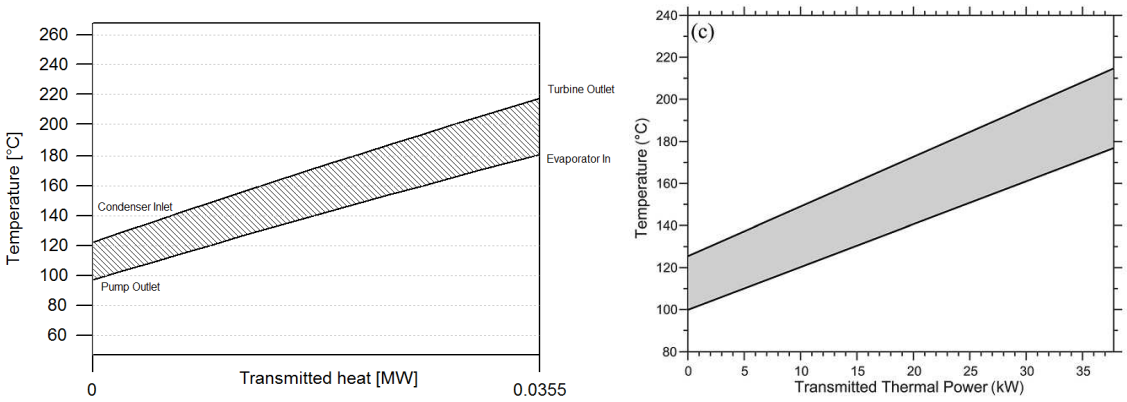

(a) Regenerator (This Work) (b) Regenerator (Lang et. al. [21])

Figure 4-13: Comparison of Q-T diagrams for regenerators

Figure 4-12 illustrates the Q-T diagrams for the condenser. The condenser temperature is imposed as 100 ^{o}C in the work of Lang et. al. [21] while it is not the case in this work. The amount of exergy lost in the condenser is relatively lower in this work. Figure 4-13 illustrates a comparison of the Q-T diagrams for the regenerator. The amount of exergy lost is arguably similar in both the cases.

The feasibility of the heat exchangers are governed mainly by the volume and the weight of these equipments. The important constraints to selection of these equipments are the pressure loss and the allowable heat exchanger volume. However, according to Lang et. al., the feasibility of the expander and the benefits of a lubricant working fluid are arguably more stringent constraints on the feasibility of the heat recovery system than the size of the heat exchangers [21]. But in order to have a practically feasible system, it is important to design the heat exchangers as these equipments tend to be comparatively more expensive than the turbine.

Chapter 5

Conclusion

5-1 Conclusion

In this work, a tool which simultaneously optimizes the working fluid and the process parameters has been developed. The tool is based on the CoMT-CAMD method as an integrated design of processes and fluids is highly desirable due to their strong interdependence. It presents a sound integration of molecular design into process optimization using the evolutionary genetic algorithm which circumvents the prohibitive complexity of the discrete choice between individual molecules. The result of the first phase of this method is an optimal process and a hypothetical working fluid. The parameters of the optimal hypothetical working fluid are mapped onto an existing fluid and the process is optimized again.

The optimization problem has been solved by using a single objective genetic algorithm with the output power as the objective function. The use of such an evolutionary algorithm leads to an a posteriori solution wherein the set of efficient candidate solutions are outlined by the algorithm from which the decision-maker chooses the solution to be used.

The use of the PCP-SAFT model provides a good description to the fluids and makes the tool versatile as it can be easily extended to mixtures and polar fluids. The segment number has been used as the fluid optimization variable and the other pure component parameters such as segment diameter and segment energy parameter have been represented in terms of the segment number. The values obtained from these expressions have been validated against the data from FluidProp. The segment energy parameter and the segment diameter derived from the polynomial fit has a certain degree of uncertainty. This can be addressed by including the segment energy and segment diameter as optimization variables for the fluid along with the segment number. A representative polynomial has been derived to predict the ideal gas heat capacity of the fluid from PCP-SAFT parameters. The polynomial predicts the ideal gas heat capacity within the uncertainty limits (5%) of the values obtained from the PCP-SAFT model.

The process has been modeled in Cycle Tempo. The tool has been tested for an ORC turbogenerator for waste heat recovery systems in heavy duty truck engines wherein the mid-grade heat available in the exhaust and the EGR system has been considered. The other

heat recovery opportunities, like power conversion from the charged air cooler and cooling systems have been considered to be too challenging for the current status of automotive heat recovery technology. The Cycle Tempo model of the turbogenerator has been validated with the model results from literature. The search space for the fluids has been limited to the family of siloxanes which not only adheres to the technical, environmental, and toxicological requirements typical of the automotive sector but also allows for the implementation of a preliminary radial turbine model, whose shaft can be lubricated by the working fluid itself.

The turbine has been modeled based on the methodology of using non-dimensional parameters, the values for which have been taken from previous work on radial turbines for gas turbines. The hypothetical optimum fluid is found to be between MM and MDM. The cycle with MDM gives an output power of 9.77 kW. The preliminary design of the ORC radial turbine resulted in a compact turbine with a rotor diameter of 7 cm and a calculated isentropic efficiency of 81.13% and high rotational speed of 66880 rpm. With MM as working fluid, although the output power is slightly higher with a value of 10.20 kW but it would require smaller turbines with high rotation speeds of about 133,858 rpm. The MM cycle also operates at a much higher pressure of around 20.73 bar. Thus the gain in output power is considerably less from MDM to MM while the high pressure and rotational speeds would mean a much more expensive system. The blade height at the rotor inlet is significantly small of the order of 1.7 mm which might have also have a negative impact on the turbine efficiency, manufacturing and operation in which case. Partial-admission is one of the possibilities to increase the blade height at the rotor inlet. The turbine model used did not influence the selection of the optimal hypothetical working fluid when compared to a turbine with constant efficiency. However, due to uncertainties in the efficiency prediction from the preliminary radial turbine model implemented and the limited fluid search space, there is not enough evidence to conclude that the turbine model does not affect the fluid selection within the optimization framework. It is important to note that the evaluation of the achievable turbine efficiency, and thus of the achievable power output of the ORC system would require experimental information on small ORC turbines, which is lacking at the moment.

The pinch point analysis function for the heat exchangers has been implemented in this tool. This has been tested on the evaporators powered by the exhaust and the EGR system. The exergy loss in the EGR evaporator is quite high in case of MDM. Additionally, the size of the condenser and regenerator are larger due to lower density of fluid from the turbine outlet. An organic working fluid made of a simpler molecule would result in a more compressed thermodynamic cycle, more compact heat exchangers, it might require a supercritical cycle configuration, and would entail a smaller and faster, and possibly far less performing single-stage turbine.

5-2 Recommendations

The search space of fluids in this work has been restricted to the family of siloxanes. Once a sufficiently detailed and accurate molecular model is available, the scope of the tool can be extended to other fluids. The segment number has been used as the only optimization variable for the fluid parameters. In case the domain of fluids is extended, the use of other pure component parameters viz. segment diameter and segment energy in addition to the segment number will yield better results. The specific heat capacity model can be improved

by using experimental data to correlate the coefficients. Furthermore, a better mapping technique needs to be developed. One possibility can be using a Taylor series approximation as shown in Chapter 2.

The costs, in particular, of the heat exchangers are a major bottleneck in realizing such a system in actual trucks. Furthermore, the optimization of only the net output power does not lead to a system with maximum heat recovery as increased levels of evaporator pressure causes a high amount of regeneration which in turn leads to a lower heat recovery from the flue gas. Thus the optimization problem can be extended to a multi-objective optimization with a Pareto frontier to arrive at an optimal solution with the output power and costs being the objectives of this process.

The preliminary radial turbine model has scope for further development. The design calculation uses values available for gas turbines in which the fluid has different properties from organic fluids. Further development of this model is possible if actual experiments are performed with organic fluids in order to acquire the required loss coefficients and other non-dimensional parameters. The design of the stator has not been included in this work. The nozzle throat opening length and throat area are limiting factors for the mass flow rate through the turbine. Furthermore, the flow is supersonic in the nozzle and hence its design is critical in order to have a shock-less turbine. Incorporation of a sophisticated computational fluid dynamics model into the same tool is not recommended at the moment as the objective of this tool should be to optimize the entire system with the working fluid and not only the turbine.

The pinch point temperature analysis in case of supercritical cycle configurations has to be developed further. One of the ways to accurately calculate the pinch point might be to evaluate the temperature difference at points where the slope of the hot and cold fluid curves is the same. Finally, a more detailed component design would lead to determination of pressure drops, heat exchanging area and volume which are also important constraints in design of a compact heat exchanger. Future studies, in general, should be devoted to further development of the system through the study of the control using dynamic models, setting up experimental test bench to validate these models.

Appendix A

Working Fluid Candidates

The following appendix presents a list of the possible working fluids applicable for ORC systems.

Category and Name	Alt. Name	P_c (bar)	T_c (^oC)
Hydrocarbons (HCs)			
Ethane	R-170	48.7	32
Propene	R-1270	45.3	91
Propane	R-290	41.8	96
Cyclopropane	HC-270	54.8	124
Propyne	-	56.3	129
Isobutane	R-600a	36.4	135
Isobutene	-	39.7	144
N-butane	R-600	37.9	152
Neopentane	-	31.6	160
Isopentane	R-601a	33.7	187
N-pentane	R-601	33.6	196
Isohexane	-	30.4	225
N-hexane	-	30.6	235
N-heptane	-	27.3	267
Cyclohexane	-	40.7	280
N-octane	-	25	296
N-nonane	-	22.7	321
N-decane	-	21	345
N-dodecane	-	17.9	382
Benzene	-	48.8	298
Toluene	-	41.3	319
p-Xylene	-	34.8	342

Ethylbenzene	-	36.1	344
N-propylbenzene	-	32	365
N-butylbenzene	-	28.9	388
Perfluorocarbons (PCFs)			
Carbon-tetrafluoride	R-14	36.8	-46
Hexafluoroethane	R-116	30.5	20
Octafluoropropane	R-218	26.8	73
Perfluoro-N-pentane	PF-5050	20.2	149
Decafluorobutane	R-3-1-10	23.2	113
Dodecafluoropentane	R-4-1-12	20.5	147
Chlorofluorocarbons (CFCs)			
Trichlorofluoromethane	R-11	43.7	197
Dichlorodifluoromethane	R-12	39.5	111
Trichlorotrifluoroethane	R-113	33.8	213
Dichlorotetrafluoroethane	R-114	32.4	145
Chloropentafluoroethane	R-115	30.8	79
Hydroflurocarbons (HFCs)			
Trifluoromethane	R-23	48.3	26
Difluoromethane	R-32	57.4	78
Fluoromethane	R-41	59	44
Pentafluoroethane	R-125	36.3	66
1,1,1,2-Tetrafluoroethane	R-134a	40.6	101
1,1,1-Trifluoroethane	R-143a	37.6	73
1,1-Difluoroethane	R-152a	44.5	112
1,1,1,2,3,3,3-Heptafluoropropane	R-227ea	28.7	101
1,1,1,3,3,3-Hexafluoropropane	R-236fa	31.9	124
1,1,1,2,3,3-Hexafluoropropane	R-236ea	34.1	139
1,1,1,3,3-Pentafluoropropane	R-245fa	36.1	153
1,1,2,2,3-Pentafluoropropane	R-245ca	38.9	174
Octafluorocyclobutane	RC-318	27.8	114
1,1,1,2,2,3,3,4-Octafluorobutane	R-338mccq	27.2	159
1,1,1,3,3-Pentafluorobutane	R-365mfc	32.7	187
Hydrofluoroolefins (HFOs)			
2,3,3,3-Tetrafluoropropene	HFO-1235yf	33.8	94.7
Hydrochloroflurocarbons (HCFCs)			
Dichlorofluoromethane	R-21	51.8	178
Chlorodifluoromethane	R-22	49.9	96
1,1-Dichloro-2,2,2-trifluoroethane	R-123	36.6	183
2-Chloro-1,1,1,2-tetrafluoroethane	R-124	36.2	122
1,1-Dichloro-1-fluoroethane	R-141b	42.1	204
1-Chloro-1,1-difluoroethane	R-142b	40.6	137
Siloxanes			
Hexamethyldisiloxane	MM	19.1	245
Octamethyltrisiloxane	MDM	14.4	291
Decamethyltetrasiloxane	MD2M	12.2	326
Dodecamethylpentasiloxane	MD3M	9.3	354
Octamethylcyclotetrasiloxane	D4	13.1	312

Decamethylcyclopentasiloxane	D5	11.6	346
Dodecamethylcyclohexasiloxane	D6	9.5	371
Alcohols			
Methanol	-	81	240
Ethanol	-	40.6	241
Fluorinated ethers			
Pentafluorodimethylether	RE125	33.6	81
Bis-difluoromethyl-ether	RE134	42.3	147
2-Difluoromethoxy-1,1,1-trifluoroethane	RE245	34.2	170
Pentafluoromethoxyethane	RE245mc	28.9	134
Heptafluoropropyl-methyl-ether	RE347mcc	24.8	165
Ethers			
Dimethyl-ether	RE170	53.7	127
Diethyl-ether	R-610	36.4	193
Inorganics			
Ammonia	R-717	113.3	132
Water	R-718	220.6	374
Carbon dioxide	R-744	73.8	31

Table A-1: Pure Working Fluid Candidates (Adapted from Bao J. and Zhao L. [64])

Appendix B

Model Details

B-1 Thermodynamic Model

The molecular mass, segment diameter and segment energy parameters have been fitted with a polynomial function in terms of the segment number. The quadratic fit for the molecular mass is given by the equation:

$$MolecularMass = -0.6761m^2 + 105.59m - 279.55 \tag{B-1}$$

The quadratic fit for the segment diameter is given by the equation:

$$\sigma = 0.0179m^2 - 0.0473m + 3.8726 \tag{B-2}$$

The quadratic fit for the segment energy parameter is given by the equation:

$$\epsilon/k = 0.4016m^2 - 1.5587m + 209.29 \tag{B-3}$$

B-2 Turbine Model

B-2-1 Nozzle Inlet

The subroutine NOZZLEIN calculates the enthalpy (total), density, volumetric flow rate, speed of sound (static and total) at the nozzle inlet which are used further in the calculation

procedure. The following relations have been used in this subroutine:

$$\begin{aligned} h_{01} &= h_1 + \frac{v_1^2}{2} \\ s_1 &= s(p_1, h_1) \\ \rho_1 &= \frac{1}{\nu(p_1, h_1)} \\ vol_{in} &= \frac{m_1}{rho_1} \\ a_1 &= a(p_1, h_1) \\ a_{01} &= a(p_0 1, s_1) \end{aligned} \tag{B-4}$$

B-2-2 Rotor Inlet

The subroutine ROTORIN calculates the enthalpies, pressure, entropy, density and speed of sound (static and total) at the rotor inlet. The nozzle is assumed to be adiabatic, hence we have:

$$h_{02} = h_{01} \tag{B-5}$$

also,

$$h_2 = h_3 + R\,(h_1 - h_4) \tag{B-6}$$

(B-7)

Hence the absolute velocity is expressed as:

$$v_2 = \sqrt{2(h_{02} - h_2)} \tag{B-8}$$

(B-9)

Using the isentropic efficiency of the nozzle,

$$h_{2is} = h_1 - \frac{h_1 - h_2}{\eta_{tsnozzle}} \tag{B-10}$$

The pressure, entropy, density and speed of sound are calculated using FluidProp handles as follows:

$$\begin{aligned} p_2 &= p(h_{2is}, s_1) \\ s_2 &= s(p_2, h_2) \\ \rho_2 &= \frac{1}{\nu(p_2, h_2)} \\ a_2 &= a(p_2, h_2) \end{aligned} \tag{B-11}$$

The absolute and relative flow angles are calculated as:

$$\alpha_2 = sin^{-1}\,(v_{t2}/v_2)\,, \quad \beta_2 = cos^{-1}\,(v_{m2}/w_2) \tag{B-12}$$

where v_{t2} and v_{m2} are the tangential and meridional (radial) components of the absolute velocity v_2. v_{t2} is calculated as:

$$C_0 = \sqrt{2(h_{01} - h_{3s})} \tag{B-13}$$
$$u_2 = \psi C_0 \tag{B-14}$$
$$v_{t2} = \frac{W}{m_1 u_2} \tag{B-15}$$

The static and stagnation Mach numbers for absolute and relative velocities are then given by:

$$\begin{aligned} M_x &= \frac{v_x}{a_x} \\ M_{0x} &= \frac{v_x}{a_{0x}} \end{aligned} \tag{B-16}$$

B-2-3 Rotor Outlet

The subroutine ROTOROUT calculates the dimensions of the turbine in addition to the enthalpies, density and speed of sound of the fluid. The enthalpy, pressure, entropy and speed of sound under total conditions is assumed to be equal to the corresponding parameters at the turbine outlet. These properties are expressed as:

$$\begin{aligned} p_3 &= p_4 \\ h_{3s} &= h(p_3, s_2) \\ \rho_3 &= \frac{1}{\nu(p_3, h_3)} \\ s_3 &= s_4 \\ a_3 &= a(p_3, h_3) \\ a_{03} &= a_{04} \end{aligned} \tag{B-17}$$

The rotor inlet diameter is calculated from the rate of mass flow as:

$$m = \rho_3 v_{m3} A_3 \tag{B-18}$$
$$D_2^2 = \frac{m}{\rho_3 \phi u_2 \pi \left(\frac{D_{3s}}{D_2}\right)^2 \left(1 - \left(\frac{D_{3h}}{D_{3s}}\right)^2\right)} \tag{B-19}$$

where the diameter ratios are defined as inputs as mentioned in Table 3-5. Once D_2 is found, the rotor outlet diameter can be calculated through the ratios which are available. The flow is assumed to have no swirl component and hence, α_3 is zero. The relative flow angle is calculated as:

$$\beta_3 = cos^{-1}\left(\frac{v_{m3}}{w_3}\right) \tag{B-20}$$

This establishes the velocity triangle and thus the Mach number can be calculated using equation B-16. One of the most important parameter is the nozzle blade height at rotor inlet.

This is calculated as follows:

$$m = \rho_2 v_{m2} PER_2 \tag{B-21}$$
$$= \rho_2 v_{m2} \pi b_2 D_2 \tag{B-22}$$
$$\therefore \quad b_2 = \frac{m}{\rho_2 v_{m2} \pi D_2} \tag{B-23}$$

where PER_2 is the perimeter at the rotor inlet. Also,

$$\frac{A_3}{A_2} = \frac{\rho_3 v_{m3}}{\rho_2 M_{m2} a_{01}} \tag{B-24}$$

B-2-4 Turbine Outlet

The subroutine TUOUTLET calculates the enthalpies, density and speed of sound of the fluid at this station. Furthermore, it determines the volumetric flow rate and temperature at the turbine exit. The stagnation enthalpy is determined by using the isentropic efficiency of the turbine given by the equation:

$$h_{04} = h_{01} - \eta_i \left(h_{01} - h_{4s}\right) \tag{B-25}$$

The optimum value of η_i is achieved when the value converges to the efficiency calculated using equation 3-13. The iterative Newton-Raphson method has been implemented to achieve the solution.

B-3 Turbine Model Variable list

Variables	Engineering Symbol\Physical Meaning	Units
	Nozzle Inlet - Station 1	
T1	Temp at inlet of nozzle	^{o}C
V1	Velocity at nozzle inlet	m/s
P1	Pin at inlet to nozzle	bar
H1	Enthalpy at inlet to nozzle	kJ/kg
H01	Total Enthalpy at 1	kJ/kg
S1	Entropy at 1	kJ/kgK
RHO1	Density at 1	kg/m^3
M1	Mass flow rate at 1	kg/s
ETATS	Total-Static efficiency	%
ETATSNOZ	Total-Static nozzle efficiency	%
R	Degree of Reaction	-
VOLIN	VolumeFlow	m3/s
A1	Speed of sound	m/s
A01	Speed of sound in total conditions	m/s
SPR	Static Pressure Ratio	-
SVR	Static Volume Ratio	-
SDH	Static enthalpy drop	kJ/kg

TDH	Total enthalpy drop	kJ/kg
POWOUT	Power Output	kW
SW	Specific Power Coefficient	-
	Nozzle Vanes	
ZB	Min Number of blades	-
ZBGLASS	Min number of blades given by Glassman(1976)	-
ZBJAM	Min number of blades given by Jamieson(1955)	-
OPALPHA2	Optimum Absolute Flow angle based on Zb	deg
OPBETA2	Optimum Relative Flow angle based on Zb	deg
	Rotor Inlet - Station 2	
H2IS	Isentropic Enthalpy at 2	kJ/kg
H2	Enthalpy at 2	kJ/kg
P2	Pressure at rotor inlet	bar
S2	Entropy at 2	kJ/kgK
RHO2	Density at 2	kg/m^3
A2	Speed of sound at 2	m/s
BETA2	Actual Relative inlet flow angle	deg
ALPHA2	Actual Absolute inlet flow angle	deg
TMV(0)	Inlet Stagnation Mach Number [v2/a01]	-
TMV(1)	Relative Mach Number [vm2/a01]	-
TMV(2)	Relative Mach Number [vt2/a01]	-
TMW(0)	Relative Mach Number [w2/a01]	-
TMU(0)	Relative Mach Number [u2/a01]	-
MV(0)	Rotor Inlet Mach Number [v2/a2]	-
MV(1)	Mach Number [vm2/a2]	-
MV(2)	Mach Number [vt2/a2]	-
MW(0)	Mach Number [w2/a2]	-
MU(0)	Mach Number [u2/a2]	-
B2R2	Blade Height to Radius ratio	-
B2	Blade Height at Rotor inlet	mm
	Rotor Outlet - Station 3	
H3IS	Isentropic Enthalpy	kJ/kg
H3	Enthalpy	kJ/kg
P3	Pressure at rotor outlet	bar
S3	Entropy	kJ/kgK
RHO3	Density	kg/m^3
A3	Speed of sound	m/s
A03	Speed of sound in total conditions	m/s
WR	Relative velocity ratio [w3s/w2]	-
DHS	Hub-shroud diameter ratio [D3h/D3s]	-
D3SD2	Ratio of shroud diameter at rotor outlet to diameter of rotor inlet	-
	At Shroud	
BETA3S	Relative out flow angle	degrees
TMW(1)	Relative Mach Number [w3s/a03]	-
TMU(1)	Relative Mach Number [u3s/a03]	-

TMW(2)	Mach Number [w3s/a01]	-
TMU(2)	Relative Mach Number [u3s/a01]	-
MW(1)	Mach Number [w3s/a3]	-
D3S	Outlet Rotor Diameter	mm
	At Hub	
TMW(3)	Relative Mach Number [w3h/a03]	-
TMW(4)	Relative Mach Number [w3h/a01]	-
TMU(3)	Relative Mach Number [u3h/a03]	-
TMU(4)	Relative Mach Number [u3h/a01]	-
BETA3H	Relative out flow angle	deg
D3H	Rotor Outlet diameter	mm
TMV(3)	Relative Mach Number [vm3/a03]	-
TMV(4)	Relative Mach Number [vm3/a01]	-
MV(3)	Mach Number [vm3/a3]	-
VM3	Meridonial component of absolute velocity	m/s
BETA3RMS	Relative out flow angle at root mean square diameter	deg
AR2AR3	Ratio of area at rotor inlet to outlet	-
D3RMS	Diameter at root mean square radii	mm
	Diffuser Outlet - Station 4	
H4IS	Isentropic Enthalpy	kJ/kg
H4	Enthalpy	kJ/kg
H04	Total Enthalpy	kJ/kg
P4	Pressure	bar
S4	Entropy	kJ/kgK
RHO4	Density	kg/m^3
A4	Speed of sound	m/s
A04	Speed of sound in total conditions	m/s
V4	Velocity at the outlet of turbine	m/s
RPM	Rotational Speed of the turbine	rpm
SD	Specific Diameter	-
SN	Specific Speed	-

Table B-1: Turbine Model Variable list

B-4 MATLAB Functions

B-4-1 Function to calculate Evaporator Temperature

```
%%%%%%%%%%%%%%%%%%%%%%%%%%%%%%%%%%%%%%%%%%%%%%%%%%%%%%%%%%%%%%%%%%%%%%%%%%%%%%%%
%                                                                               %
%                          FUNCTION GETDATA                                     %
%                           ---------------                                     %
%                                                                               %
% DESCRIPTION : CALCULATES THE EVAPORATOR TEMPERATURE REQUIRED AS INPUT         %
%               TO CYCLE TEMPO CALCULATION                                      %
% NO.         : 1.0                                                             %
%                                                                               %
```

```
% DATE         : 26-05-2013                                                %
%                                                                          %
% INPUTS       : rqst:- Track  the  evaluation  request in Nexus           %
%                ins :- Inputs (Evaporator Pressure) as per Nexus          %
%                outs:- Outputs(Evaporator Temperature) as per Nexus       %
% CALLED BY    : Nexus Matlab module                                       %
%%%%%%%%%%%%%%%%%%%%%%%%%%%%%%%%%%%%%%%%%%%%%%%%%%%%%%%%%%%%%%%%%%%%%%%%%

function [outs] = GetData(rqst,ins,outs)

 P_Evap(rqst.objectId) = ins(1).value;
 fluid = 'DORC';
 ext='.saf';
 fplocation = 'C:\Program Files (x86)\FluidProp\';
 fluidtab = ins(2).value;
 status(rqst.objectId) = ins(3).value;
 y = rqst.requestId-1;

if(status(rqst.objectId) == 0)

            %% Copy Fluid Files into FP folder
            % dirlocation: Create unique location for each run
            dirlocation = strcat(rqst.homeDir,'nxRuns\nxRun_oid' ,...
                num2str(rqst.objectId),'_s',num2str(rqst.schedulerId) ,...
                '_r',num2str(y),'\');
            % fluidfile: Unique fluid file based on object id
            fluidfile = strcat(fluid,'_',num2str(rqst.objectId),ext);
            %newfilename
            fluidsource = strcat(dirlocation,fluidfile);
            %oldfilename
            localdestination = strcat(dirlocation,'DORC.saf');
            %renamefile
            movefile(localdestination,fluidsource);
            %FluidProp directory
            destination = strcat(fplocation,fluidfile);
            [stat] = copyfile(fluidsource,destination,'f');
            Cmp(rqst.objectId)   = {strcat(fluid,'_' ,...
                                    num2str(rqst.objectId))};
 end
 if (status(rqst.objectId) == 1)
            dirlocation = strcat(rqst.homeDir,'nxRuns\nxRun_oid' ,...
                num2str(rqst.objectId),'_s',num2str(rqst.schedulerId) ,...
                '_r',num2str(y),'\');
            fluidfile = strcat(fluid,ext); %without objectid
            %newfilename
            fluidsource = strcat(dirlocation,fluidfile);
            %FluidProp directory
            destination = strcat(fplocation,fluidfile);
             [stat] = copyfile(fluidsource,destination,'f');
             Cmp(rqst.objectId)   = {fluid};
 end


```

```
%% Compute Evaporator Temperature
 outs(1).value =0;
 nCmp  = 1;
 Cnc   = [1,0];
 Model = 'PCP-SAFT';
 if ((P_Evap == -1) || (stat ~= 1))
      T_Evap(rqst.objectId) = -1;
 else
        FP(rqst.objectId) = actxserver('FluidProp.FluidProp'); %Create FP
            COM server
        Cmp(rqst.objectId)   = {strcat(fluid,'_',num2str(rqst.objectId))
            };
        ErrorMsg = invoke(FP(rqst.objectId),'SetFluid_M',Model,nCmp,Cmp
            {1,rqst.objectId},Cnc);
        P_c(rqst.objectId) = FP(rqst.objectId).Pcrit;
        T_c(rqst.objectId) = FP(rqst.objectId).Tcrit;
         if((P_c(rqst.objectId))&&(T_c(rqst.objectId)))
           [v_c(rqst.objectId), ErrorMsg]=invoke(FP(rqst.objectId),'
               SpecVolume','PT',P_c(rqst.objectId),T_c(rqst.objectId));
           [Tsat(rqst.objectId), ErrorMsg2] = invoke(FP(rqst.objectId),'
               Temperature','Pv',P_Evap,v_c(rqst.objectId));
           if (strcmpi(ErrorMsg,'No errors') == 0) || (strcmpi(ErrorMsg2,
               'No errors') == 0)
                 T_Evap(rqst.objectId) = -1; % returns -1 if calculation
                     does not converge
           else
                 T_Evap(rqst.objectId) = Tsat(rqst.objectId) + 5;
           end
         else
                 T_Evap(rqst.objectId) = 0;
         end
end

outs(1).value = T_Evap(rqst.objectId);
outs(1).status = 0;
outs(2).value = rqst.objectId;
outs(2).status = 0;
outs(3).value = rqst.requestId;
outs(3).status = 0;
outs(4).value = rqst.schedulerId;
outs(4).status = 0;
outs(5).value = rqst.homeDir;
outs(5).status = 0;
outs(6).value = x;
outs(6).status = 0;
outs(7).value =  fluidsource;
outs(7).status = 0;


end
```

B-4-2 Function to calculate Pinch Point Temperature Difference

```
%%%%%%%%%%%%%%%%%%%%%%%%%%%%%%%%%%%%%%%%%%%%%%%%%%%%%%%%%%%%%%%%%%%%%%%%%%%%%%%%
%                                                                                 %
%                          FUNCTION PINCHPOINT                                    %
%                             ---------------                                     %
%                                                                                 %
%   DESCRIPTION : CALCULATES THE PINCH POINT TEMPERATURE DIFFERENCE               %
%                 FOR THE EXHAUST GAS AND EGR EVAPORATORS                         %
%   NO.         : 1.0                                                             %
%                                                                                 %
%   DATE        : 26-05-2013                                                      %
%                                                                                 %
%   INPUTS      : rqst:- Track  the  evaluation  request in Nexus                 %
%                 ins :- Inputs as per Nexus                                      %
%                        Evaporator Pressure                                      %
%                        Lower temperature difference                             %
%                        (WF Inlet and FG outlet)                                 %
%                        Evaporator outlet temperature - WF side                  %
%                        EGR HX - FlueGas inlet temperature                       %
%                        Exhaust HX - FlueGas inlet temperature                   %
%                        Mass flow rate of working fluid in EGR HX                %
%                        Mass flow rate of working fluid in Exhaust HX            %
%                        Mass flow rate of flue gas in the EGR HX                 %
%                        Mass flow rate of flue gas in the Exhaust HX             %
%                        Evaporator inlet temperature- WF side                    %
%                        Exhaust HX exit tempetaure - FlueGas side                %
%                        EGR HX Exit temperature - FlueGas side                   %
%                                                                                 %
%                 outs:- Outputs as per Nexus                                     %
%                        Exhaust HX Pinch point temperature difference            %
%                        EGR HX Pinch point temperature difference                %
%   CALLED BY   : Nexus Matlab module                                             %
%%%%%%%%%%%%%%%%%%%%%%%%%%%%%%%%%%%%%%%%%%%%%%%%%%%%%%%%%%%%%%%%%%%%%%%%%%%%%%%%
%            Exhaust/EGR in                                                       %
%            T_Ex1/T_EGR1 W_Ex/W_Egr                                              %
%            -------------                                                        %
%          |             |                                                        %
%          |             |                                                        %
%          |    _   _    |                                                        %
% WFin     |___/ \_/ \___| WF out                                                 %
% T_Evapin |             |T_Evap M_Ex/M_Egr                                       %
%       ____|             |                                                       %
%      |    |_____________|                                                       %
%     DELT   Exhaust/EGR out                                                      %
%      |____ T_Ex2/T_EGR2                                                       %
%%%%%%%%%%%%%%%%%%%%%%%%%%%%%%%%%%%%%%%%%%%%%%%%%%%%%%%%%%%%%%%%%%%%%%%%%%%%%%%%
function [outs] = PinchPoint(rqst,ins,outs)
%% Initialize all the variables

P_Evap(rqst.objectId)   = 0; % Evaporator Pressure
DELTL(rqst.objectId)    = 0; % Lower temperature difference
                             % (WF Inlet and FG outlet)
T_Evap(rqst.objectId)   = 0; % Evaporator outlet temperature - WF side
T_Egr1(rqst.objectId)   = 0; % EGR HX - FlueGas inlet temperature
```

```
54 T_Ex1(rqst.objectId)     = 0; % Exhaust HX - FlueGas inlet temperature
55 M_Egr(rqst.objectId)     = 0; % Mass flow rate of working fluid
56                               % in EGR HX
57 M_Ex(rqst.objectId)      = 0; % Mass flow rate of working fluid
58                               % in Exhaust HX
59 W_Egr(rqst.objectId)     = 0; % Mass flow rate of flue gas
60                               % in the EGR HX
61 W_Ex(rqst.objectId)      = 0; % Mass flow rate of flue gas
62                               % in the Exhaust HX
63 T_Evapin(rqst.objectId) = 0; % Evaporator inlet temperature-WF side
64 T_Ex2(rqst.objectId)     = 0; % Exhaust HX exit tempetaure-FlueGas side
65 T_Egr2(rqst.objectId)    = 0; % EGR HX Exit temperature-FlueGas side
66 oid = rqst.objectId;
67 P_atm(rqst.objectId) = 1.01325; % Pressure on fluegas side in bar
68
69 check = zeros(1,rqst.objectId);
70  for i=1:10
71      if(ins(i).value==-1)
72          check(rqst.objectId) = -1;
73          T_PinchEx(rqst.objectId) = -1;
74          T_PinchEGR(rqst.objectId) = -1;
75          h_WF1(rqst.objectId)=-1;
76          h_WFsat1(rqst.objectId)=-1;
77          h_Ex2(rqst.objectId)=-1;
78          h_Egr2(rqst.objectId)=-1;
79          dh_Ex(rqst.objectId) = -1;
80          dh_Egr(rqst.objectId) = -1;
81          T_ExY(rqst.objectId)=-1;
82          T_EgrY(rqst.objectId)=-1;
83          break;
84      end
85  end
86 %%   For valid inputs
87  if(check(rqst.objectId)== 0)
88     P_Evap(rqst.objectId) = ins(1).value;
89     DELTL(rqst.objectId) = ins(2).value;
90     T_Egr1(rqst.objectId) = ins(3).value;
91     T_Ex1(rqst.objectId)  = ins(4).value;
92     M_Egr(rqst.objectId) = ins(5).value;
93     M_Ex (rqst.objectId) = ins(6).value;
94     W_Egr(rqst.objectId)  = ins(7).value;
95     W_Ex (rqst.objectId) = ins(8).value;
96     T_Evapin(rqst.objectId) = ins(9).value;
97     aid (rqst.objectId) = ins(10).value;
98     x (rqst.objectId) = ins(11).value;
99     T_Evap (rqst.objectId)= ins(12).value;
100    fluid = strcat('DORC_',num2str(oid));
101    T_Ex2(rqst.objectId) = T_Evapin(rqst.objectId)+ DELTL(rqst.objectId);
102    T_Egr2(rqst.objectId)= T_Evapin(rqst.objectId)+ DELTL(rqst.objectId);
103    % Saturated temperature is fixed to be 5 K lower than
104    % evaporator outlet temperature
105    T_sat(rqst.objectId) = T_Evap(rqst.objectId)- 5;
106     if(P_Evap(rqst.objectId) > x(rqst.objectId))
```

```
107       %% Supercritical
108         dTWF (rqst.objectId)     = 0;
109         dTFG_EX(rqst.objectId)   = 0;
110         T_ExFG   = zeros(rqst.objectId,100);
111         T_EgrFG  = zeros(rqst.objectId ,100);
112         T_WF     = zeros(rqst.objectId ,100);
113         dTWF(rqst.objectId)      = (T_Evap(rqst.objectId) -...
114                                     T_Evapin(rqst.objectId))/99;
115         dTFG_EX(rqst.objectId)   = (T_Ex1(rqst.objectId) -...
116                                     T_Ex2(rqst.objectId))/99;
117         dTFG_EGR(rqst.objectId) = (T_Egr1(rqst.objectId) -...
118                                     T_Egr2(rqst.objectId))/99;
119         T_ExFG(rqst.objectId,1) = T_Ex1(rqst.objectId);
120         T_EgrFG(rqst.objectId,1)= T_Egr1(rqst.objectId);
121         T_WF(rqst.objectId,1)   = T_Evapin(rqst.objectId);
122         for i = 1:99
123            T_ExFG(rqst.objectId,i+1)  = T_ExFG(rqst.objectId,i)...
124                                         - dTFG_EX(rqst.objectId);
125            T_EgrFG(rqst.objectId,i+1) = T_EgrFG(rqst.objectId,i)...
126                                         - dTFG_EGR(rqst.objectId);
127            T_WF(rqst.objectId,i+1)    = T_WF(rqst.objectId,i)...
128                                         + dTWF(rqst.objectId);
129         end
130         T_PinchEx(rqst.objectId) = min(abs(T_ExFG(rqst.objectId,:)...
131                                    - T_WF(rqst.objectId,:) ));
132         T_PinchEGR(rqst.objectId)= min(abs(T_ExFG(rqst.objectId,:)...
133                                    - T_WF(rqst.objectId,:) ));
134         if ((T_PinchEx(rqst.objectId) > T_Evapin(rqst.objectId))...
135             ||(T_PinchEGR(rqst.objectId) > T_Evapin(rqst.objectId)))
136              T_PinchEx(rqst.objectId) = -1;
137              T_PinchEGR(rqst.objectId)= -1;
138         end
139 %          Not required for super critical
140         h_WF1(rqst.objectId)=-5;
141         h_WFsat1(rqst.objectId)=-5;
142         h_Ex2(rqst.objectId)=-5;
143         h_Egr2(rqst.objectId)=-5;
144         dh_Ex(rqst.objectId) = -5;
145         dh_Egr(rqst.objectId) = -5;
146         T_ExY(rqst.objectId)=-5;
147         T_EgrY(rqst.objectId)=-5;
148       else
149          %% Sub-critical
150          %Create FP COM server
151          FP_WF(rqst.objectId) = actxserver('FluidProp.FluidProp');
152          FP_FG(rqst.objectId) = actxserver('FluidProp.FluidProp');
153          nCmp_WF = 1; % Number of components in working fluid
154          q=0; % Pure liquid
155          r=1; % Pure vapor
156          nCmp_FG = 4; % Number of components in Flue gas
157          Cnc_WF  = [1,0]; % Concentration of working fluid components
158          Cmp(rqst.objectId) = {fluid}; % Component Fluid
159          % Bombarda, 2010
```

```
160         % Components of Flue Gas
161         Cmp_FG     = 'Ar,CO2,H2O,N2,O2';
162         % Concentration of each component
163         Cnc_FG  = [0.011,0; 0.059,0; 0.0670,0; 0.7460,0;0.117,0];
164         Model_WF = 'PCP-SAFT';
165         Model_FG = 'GASMIX';
166         % WF uses PCP-SAFT model while FG uses GASMIX
167
168 %% FG Heat Flow
169         ErrorMsg = invoke(FP_FG(rqst.objectId),'SetFluid_M',Model_FG...
170                           ,nCmp_FG,Cmp_FG,Cnc_FG); %Fluegas
171         [h_Ex2(rqst.objectId),ErrorMsg] = invoke(FP_FG(rqst.objectId)...
172            ,'Enthalpy','PT',P_atm(rqst.objectId), T_Ex2(rqst.objectId));
173         [h_Egr2(rqst.objectId),ErrorMsg] = invoke(FP_FG(rqst.objectId)...
174           ,'Enthalpy','PT',P_atm(rqst.objectId), T_Egr2(rqst.objectId));
175 %%   WF Heat Flow
176         ErrorMsg = invoke(FP_WF(rqst.objectId),'SetFluid_M',Model_WF...
177                      ,nCmp_WF,Cmp{1,rqst.objectId},Cnc_WF);
178
179         [h_WF1(rqst.objectId), ErrorMsg2]= invoke(FP_WF(rqst.objectId)
               ,...
180           'Enthalpy','PT',P_Evap(rqst.objectId),T_Evapin(rqst.objectId));
181         [h_WFsat1(rqst.objectId),ErrorMsg]=invoke(FP_WF(rqst.objectId)...
182            ,'Enthalpy','Pq',P_Evap(rqst.objectId),q);
183         [h_WFsat2(rqst.objectId),ErrorMsg]=invoke(FP_WF(rqst.objectId)...
184            ,'Enthalpy','Pq',P_Evap(rqst.objectId),r);
185         [h_WF2(rqst.objectId),ErrorMsg]= invoke(FP_WF(rqst.objectId)...
186            ,'Enthalpy','PT',P_Evap(rqst.objectId),T_Evap(rqst.objectId));
187
188         Qpre_Ex(rqst.objectId) = M_Ex(rqst.objectId)*...
189                       (h_WFsat1(rqst.objectId)-h_WF1(rqst.objectId));
190
191         Qpre_Egr(rqst.objectId)= M_Egr(rqst.objectId)*...
192                       (h_WFsat1(rqst.objectId)-h_WF1(rqst.objectId));
193
194 %% Heat balance in before saturation in Exhaust Hx
195        dh_Ex(rqst.objectId) = Qpre_Ex(rqst.objectId)/W_Ex(rqst.objectId);
196        h_ExY(rqst.objectId) = h_Ex2(rqst.objectId)+ dh_Ex(rqst.objectId);
197        T_ExY(rqst.objectId) = invoke(FP_FG(rqst.objectId) ,...
198            'Temperature','Ph',P_atm(rqst.objectId),h_ExY(rqst.objectId));
199        T_PinchEx(rqst.objectId) = T_ExY(rqst.objectId)...
200                                    - T_sat(rqst.objectId);
201
202 %% Heat balance in before saturation in EGR Hx
203
204      dh_Egr(rqst.objectId)= Qpre_Egr(rqst.objectId)/W_Egr(rqst.objectId);
205      h_EgrY(rqst.objectId)= h_Egr2(rqst.objectId)+ dh_Egr(rqst.objectId);
206      T_EgrY(rqst.objectId)= invoke(FP_FG(rqst.objectId) ,...
207          'Temperature','Ph',P_atm(rqst.objectId),h_EgrY(rqst.objectId));
208      T_PinchEGR(rqst.objectId) = T_EgrY(rqst.objectId)...
209                                   -T_sat(rqst.objectId);
210 %%  Release FluidProp objects
211      invoke(FP_WF(rqst.objectId),'ReleaseObjects');
```

```
212         delete(FP_WF(rqst.objectId));
213         invoke(FP_FG(rqst.objectId),'ReleaseObjects');
214         delete(FP_FG(rqst.objectId));
215         end
216  end
217 outs(1).value = min(T_PinchEx(rqst.objectId),DELTL(rqst.objectId));
218 outs(1).status = 0;
219 outs(2).value = min(T_PinchEGR(rqst.objectId),DELTL(rqst.objectId));
220 outs(2).status = 0;
221 outs(3).value = num2str(oid);
222 outs(3).status = 0;
223 outs(4).value = h_WF1(rqst.objectId);
224 outs(4).status = 0;
225 outs(5).value = h_WFsat1(rqst.objectId);
226 outs(5).status = 0;
227 outs(6).value = h_Ex2(rqst.objectId);
228 outs(6).status = 0;
229 outs(7).value = h_Egr2(rqst.objectId);
230 outs(7).status = 0;
231 outs(8).value = dh_Ex(rqst.objectId);
232 outs(8).status = 0;
233 outs(9).value = dh_Egr(rqst.objectId);
234 outs(9).status = 0;
235 outs(10).value = T_ExY(rqst.objectId);
236 outs(10).status = 0;
237 outs(11).value = T_EgrY(rqst.objectId);
238 outs(11).status = 0;
239 end
```

Bibliography

[1] A. Whitfield and N. C. Baines, *Design of Radial Turbomachines*. Longman Scientific and Technical, Harlow, England, 1990.

[2] D. Carrington, "Global carbon dioxide in atmosphere passes milestone level." Guardian UK, 2013.

[3] F. Vélez, J. Segovia, M. Martín, G. Antolín, F. Chejne, and A. Quijano, "A technical, economical and market review of Organic Rankine Cycles for the conversion of low-grade heat for power generation," *Renewable and Sustainable Energy Reviews*, vol. 16, no. 6, pp. 4175–4189, 2012.

[4] S. Evans, "German coal power revival poses new emissions threat," August 2012.

[5] M. Lampe, J. Gross, and A. Bardow, "Simultaneous process and working fluid optimization for Organic Rankine Cycles (ORC) using PC-SAFT," in *Proceedings og the 22nd European Symposium on Computer Aided Process Engineering, London* (M. F. Ian David Lockhart Bogle, ed.), Elsevier, 2012.

[6] S. Quoilin, M. V. D. Broek, S. Declaye, P. Dewallef, and V. Lemort, "Techno-economic survey of Organic Rankine Cycle (ORC) systems," *Renewable and Sustainable Energy Reviews*, vol. 22, pp. 168–186, 2013.

[7] F. A. DiBella, L. R. DiNanno, and M. D. Koplow, "Laboratory and on-highway testing of diesel Organic Rankine compound long-haul vehicle engine," tech. rep., 1983.

[8] T. P. van der Stelt, N. Woudstra, and P. Colonna, "Cycle-Tempo: a program for the thermodynamic analysis and optimization of systems for the production of electricity, heat and refrigeration," *Energy Technology Section, Delft University of Technology, NL*, 2002.

[9] G. Angelino, M. Gaia, and E. Macchi, "A review of Italian activity in the field of Organic Rankine Cycles," *VDI-Berichte*, no. 539, pp. 465–482, 1984.

[10] I. Vankeirsbilck, B. Vanslambrouck, S. Gusev, and M. De Paepe, "Organic Rankine Cycle as efficient alternative to steam cycle for small scale power generation," in *Proceedings of 8th International Conference on Heat Transfer, Fluid Mechanics and Thermodynamics, Pointe Aux Piments (Mauritius)*, pp. 11–13, 2011.

[11] B. F. Tchanche, G. Lambrinos, A. Frangoudakis, and G. Papadakis, "Low-grade heat conversion into power using Organic Rankine cycles–A review of various applications," *Renewable and Sustainable Energy Reviews*, vol. 15, no. 8, pp. 3963–3979, 2011.

[12] H. Chen, D. Y. Goswami, and E. K. Stefanakos, "A review of thermodynamic cycles and working fluids for the conversion of low-grade heat," *Renewable and Sustainable Energy Reviews*, vol. 14, no. 9, pp. 3059–3067, 2010.

[13] A. Papadopoulos, M. Stijepovic, and P. Linke, "On the systematic design and selection of optimal working fluids for Organic Rankine Cycles," *Applied thermal engineering*, vol. 30, no. 6, pp. 760–769, 2010.

[14] A. Papadopoulos, M. Stijepovic, P. Linke, P. Seferlis, and S. Voutetakis, "Power Generation from Low Enthalpy Geothermal Fields by Design and Selection of Efficient Working Fluids for Organic Rankine Cycles," *CHEMICAL ENGINEERING*, vol. 21, 2010.

[15] A. Papadopoulos, M. Stijepovic, P. Linke, P. Seferlis, and S. Voutetakis, "Multi-level Design and Selection of Optimum Working Fluids and ORC Systems for Power and Heat Cogeneration from Low Enthalpy Renewable Sources," in *Proceedings og the 22nd European Symposium on Computer Aided Process Engineering, London* (M. F. Ian David Lockhart Bogle, ed.), Elsevier, 2012.

[16] A. Bardow, K. Steur, and J. Gross, "Continuous-molecular targeting for integrated solvent and process design," *Industrial & Engineering Chemistry Research*, vol. 49, no. 6, pp. 2834–2840, 2010.

[17] S. L. Dixon and C. Hall, *Fluid mechanics and thermodynamics of turbomachinery.* Butterworth-Heinemann, 2005.

[18] J. Gross and G. Sadowski, "Perturbed-chain SAFT: An equation of state based on a perturbation theory for chain molecules," *Industrial & engineering chemistry research*, vol. 40, no. 4, pp. 1244–1260, 2001.

[19] J. Gross, "An equation-of-state contribution for polar components: Quadrupolar molecules," *AIChE journal*, vol. 51, no. 9, pp. 2556–2568, 2005.

[20] iChrome Ltd., "Nexus optimization suite version 2.1.0," 2013.

[21] W. Lang, P. Colonna, and R. Almbauer, "Assessment of Waste Heat Recovery From a Heavy-Duty Truck Engine by Means of an ORC Turbogenerator," *Journal of Engineering for Gas Turbines and Power*, vol. 135, pp. 042313–1, 2013.

[22] S. Macchietto, O. Odele, and O. Omatsone, "Design on optimal solvents for liquid-liquid extraction and gas absorption processes," *Chemical engineering research & design*, vol. 68, no. 5, pp. 429–433, 1990.

[23] F. E. Pereira, E. Keskes, A. Galindo, G. Jackson, and C. S. Adjiman, "Integrated design of CO2 capture processes from natural gas," *Process Systems Engineering: Energy Systems Engineering, Volume 5*, pp. 231–248, 2008.

[24] J. Wang, Z. Yan, M. Wang, M. Li, and Y. Dai, "Multi-objective optimization of an Organic Rankine Cycle (ORC) for low grade waste heat recovery using evolutionary algorithm," *Energy Conversion and Management*, vol. 71, pp. 146–158, 2013.

[25] J. Gross and J. Vrabec, "An equation-of-state contribution for polar components: Dipolar molecules," *AIChE journal*, vol. 52, no. 3, pp. 1194–1204, 2006.

[26] J. Vrabec and J. Gross, "Vapor-Liquid Equilibria Simulation and an Equation of State Contribution for Dipole-Quadrupole Interactions," *The Journal of Physical Chemistry B*, vol. 112, no. 1, pp. 51–60, 2008. PMID: 18072758.

[27] B. Oyarzún, A. Bardow, and J. Gross, "Integration of process and solvent design towards a novel generation of CO2 absorption capture systems," *Energy Procedia*, vol. 4, pp. 282 – 290, 2011. 10th International Conference on Greenhouse Gas Control Technologies.

[28] A. Uusitalo, T. Turunen-Saaresti, J. Honkatukia, P. Colonna, and J. Larjola, "Siloxanes as Working Fluids for Mini-ORC Systems Based on High-Speed Turbogenerator Technology," *Journal of Engineering for Gas Turbines and Power*, vol. 135, pp. 042305–1, 2013.

[29] G. Angelino and C. Invernizzi, "Cyclic methylsiloxanes as working fluids for space power cycles," *Journal of Solar Energy Engineering;(United States)*, vol. 115, no. 3, 1993.

[30] C. Invernizzi, P. Iora, and P. Silva, "Bottoming micro-Rankine cycles for micro-gas turbines," *Applied Thermal Engineering*, vol. 27, no. 1, pp. 100–110, 2007.

[31] E. Lodwig, *Performance of a 35 Hp Organic Rankine Cycle Exhaust Gas Powered System*. Society of Automotive Engineers, 1970.

[32] E. Doyle, L. DiNanno, and S. Kramer, "Installation of a diesel-organic Rankine compound engine in a class 8 truck for a single-vehicle test," tech. rep., 1979.

[33] P. S. Patel and E. F. Doyle, "Compounding the truck diesel engine with an Organic Rankine-cycle system," tech. rep., 1976.

[34] O. B. Platell, "Progress of Saab Scania's steam power project," tech. rep., 1976.

[35] H. Teng, G. Regner, and C. Cowland, "Waste heat recovery of heavy-duty diesel engines by Organic Rankine cycle part I: hybrid energy system of diesel and Rankine engines," *SAE paper*, pp. 01–0537, 2007.

[36] H. Teng, G. Regner, and C. Cowland, "Waste Heat Recovery of heavy-Duty Diesel Engines by organic Rankine Cycle part II: Working fluids for WHRORC," *SAE paper*, no. 2007-01, p. 0543, 2007.

[37] P. Colonna and T. Van der Stelt, "Fluidprop: a program for the estimation of thermo physical properties of fluids," *Energy Technology Section, Delft University of Technology, The Netherlands*, 2004.

[38] P. Bombarda, C. M. Invernizzi, and C. Pietra, "Heat recovery from Diesel engines: A thermodynamic comparison between Kalina and ORC cycles," *Applied Thermal Engineering*, vol. 30, no. 2, pp. 212–219, 2010.

[39] V. K. I. for Fluid Dynamics, "Closed Cycle Gas Turbines: Lecture Series Held At Rhode Saint Genèse," 1977.

[40] E. Sauret and A. S. Rowlands, "Candidate radial-inflow turbines and high-density working fluids for geothermal power systems," *Energy*, vol. 36, no. 7, pp. 4460–4467, 2011.

[41] B. F. Rafi, "Radial Turbine," *GRABCAD. Retrieved May*, 2012.

[42] C. Rodgers and R. Geiser, "Performance of a high-efficiency radial/axial turbine," *J. Turbomach.;(United States)*, vol. 109, no. 2, 1987.

[43] J. P. van Buijtenen, J. Larjola, T. Turunen-Saaresti, E. H. Honkatukia, J., J. Backman, and A. Reunanen, "Design and Validation of a New High Expansion Ratio Radial Turbine for ORC Application," in *Proceedings of 5th European Conference on Turbomachinery, Prague, Czech Republic, March 17-22*, 2003.

[44] D. Fiaschi, G. Manfrida, and F. Maraschiello, "Thermo-fluid dynamics preliminary design of turbo-expanders for ORC cycles," *Applied Energy*, vol. 97, pp. 601–608, 2012.

[45] H. E. Rohlik, "Analytical determination of radial inflow turbine design geometry for maximum efficiency," 1968.

[46] O. Balje, *Turbomachines - A Guide to Design Selection and Theory*. Wiley-Interscience Publication, 1981.

[47] R. S. Benson, "A review of methods for assessing loss coefficients in radial gas turbines," *International Journal of Mechanical Sciences*, vol. 12, no. 10, pp. 905–932, 1970.

[48] V. Maizza and A. Maizza, "Unconventional working fluids in Organic Rankine-cycles for waste energy recovery systems," *Applied Thermal Engineering*, vol. 21, no. 3, pp. 381–390, 2001.

[49] T. Yamamoto, T. Furuhata, N. Arai, and K. Mori, "Design and testing of the Organic Rankine Cycle," *Energy*, vol. 26, no. 3, pp. 239 – 251, 2001.

[50] J. M. Calm and D. A. Didion, "Trade-offs in refrigerant selections: past, present, and future," *International Journal of Refrigeration*, vol. 21, no. 4, pp. 308–321, 1998.

[51] A. Kazakov, M. O. McLinden, and M. Frenkel, "Computational Design of New Refrigerant Fluids Based on Environmental, Safety, and Thermodynamic Characteristics," *Industrial & Engineering Chemistry Research*, vol. 51, no. 38, pp. 12537–12548, 2012.

[52] M. Whelan, E. Estrada, and R. Van Egmond, "A modelling assessment of the atmospheric fate of volatile methyl siloxanes and their reaction products," *Chemosphere*, vol. 57, no. 10, pp. 1427–1437, 2004.

[53] E. F. Griessbach and R. Lehmann, "Degradation of polydimethylsiloxane fluids in the environmentŮa review," *Chemosphere*, vol. 38, no. 6, pp. 1461–1468, 1999.

[54] iChrome Ltd., "Keyword manual for nexus optimization suite version 2.1.0," 2013.

[55] I. StatSoft, "Electronic statistics textbook," *StatSoft, Tulsa, OK*, 2007.

[56] G. A. Kochenberger *et al.*, *Handbook in Metaheuristics*. Springer, 2003.

[57] R. T. Marler and J. S. Arora, "Survey of multi-objective optimization methods for engineering," *Structural and multidisciplinary optimization*, vol. 26, no. 6, pp. 369–395, 2004.

[58] R. A. Van den Braembussche, "Numerical optimization for advanced turbomachinery design," in *Optimization and computational fluid dynamics*, pp. 147–189, Springer, 2008.

[59] MATLAB, "version 7.11.2 (R2010bSP2)," 2010.

[60] N. Nannan, P. Colonna, C. Tracy, R. Rowley, and J. Hurly, "Ideal-gas heat capacities of dimethylsiloxanes from speed-of-sound measurements and ab initio calculations," *Fluid phase equilibria*, vol. 257, no. 1, pp. 102–113, 2007.

[61] P. Imoberdorf, C. Zwyssig, S. Round, and J. Kolar, "Combined radial-axial magnetic bearing for a 1 kW, 500,000 rpm permanent magnet machine," in *Applied Power Electronics Conference, APEC 2007-Twenty Second Annual IEEE*, pp. 1434–1440, IEEE, 2007.

[62] A. J. Glassman, "Computer program for design analysis of radial-inflow turbines," 1976.

[63] P. Colonna, J. Harinck, S. Rebay, and A. Guardone, "Real-gas effects in Organic Rankine cycle turbine nozzles," *Journal of Propulsion and Power*, vol. 24, no. 2, pp. 282–294, 2008.

[64] J. Bao and L. Zhao, "A review of working fluid and expander selections for Organic Rankine Cycle," *Renewable and Sustainable Energy Reviews*, vol. 24, pp. 325–342, 2013.

Glossary

List of Acronyms

ppm	parts per million
ORC	Organic Rankine Cycle
CAMD	Computer Aided Molecular Design
CoMT-CAMD	Continuous Molecular Targeting approach to CAMD
WHR	Waste Heat Recovery
CHP	Combined Heat and Power
PCP-SAFT	Perturbed Chain Polar-Statistical Associating Fluid Theory
EOS	equation of state
GA	Genetic Algorithm
SOGA	Single Objective Genetic Algorithm
D4	Octamethylcyclotetrasiloxane, $C_8H_{24}O_4Si_4$
D5	Decamethylcyclopentasiloxane, $C_{10}H_{30}O_5Si_5$
D6	Dodecamethylcyclohexasiloxane,$C_{12}H_{36}Si_6O_6$
MDM	Octamethyltrisiloxane, $C_8H_{24}Si_3O_2$
MD2M	Decamethyltetrasiloxane, $C_{10}H_{30}Si_4O_3$
MD3M	Dodecamethylpentasiloxane, $C_{12}H_{36}Si_5O_4$
MD4M	Tetradecamethylhexasiloxane, $C_{14}H_{42}O_5Si_6$
MM	Hexamethyldisiloxane, $C_6H_{18}OSi_2$

List of Symbols

A	Helmholtz free energy, Coefficient of ideal gas heat capacity
B	Coefficient of ideal gas heat capacity
c	Elements of the correlation matrix
C	Coefficient of ideal gas heat capacity
Cp	Ideal gas heat capacity
$\mathbf{C}_o$	Spouting velocity
C	Absolute flow velocity
D	Coefficient of ideal gas heat capacity, Rotor diameter
h	Enthalpy
L	Axial Length in the rotor
m	Segment Number
Q	Quadrapole moment
R	Degree of Reaction
S	Fitness Entropy
T	Temperature
U	Rotor Tip speed
v	Absolute flow velocity
w	Relative flow velocity
$\mathbf{Z}_B$	Number of vanes
α	Absolute flow angle
β	Relative flow angle
ΔW	Specific turbine work
ϵ_i^{AB}/k	Association Energy
ϵ_i/k	Dispersive attraction
ζ	Loss coefficient
η_{nozzle}	Nozzle isentropic efficiency
η_{ts}	Turbine isentropic efficiency
κ_i^{AB}	Association volume
μ_i	Point dipole moment
σ	Segment Diameter
ϕ	Flow Coefficient, Exit Velocity Ratio
ψ	Blade Loading Coefficient, Spouting Velocity Ratio

Subscripts

0	Stagnation (or Total)
1	Nozzle Inlet
2	Rotor Inlet
3	Rotor Outlet
4	Turbine Outlet
m	Meridonal direction
t	Tangential direction
h	Hub

s	Shroud, isentropic
rms	Root mean square distance
N	Nozzle
R	Rotor